The RHIC Cold QCD Plan for 2024 to 2028
Completing the RHIC Science Mission

Authors for the RHIC SPIN Collaboration*

Elke-Caroline Aschenauer[1], Alexander Bazilevsky[1], Xiaoxuan Chu[1], Oleg Eyser[1], Renee Fatemi[3], Carl Gagliardi[4], Ting Lin[5], Jae D. Nam[6], Ralf Seidl[7], Caroline Riedl[8], and Scott Wissink[9]

[1] *Brookhaven National Laboratory, Upton, New York 11973*
[3] *University of Kentucky, Lexington, Kentucky 40506-0055*
[4] *Texas A&M University, College Station, Texas 77843*
[5] *Shandong University, Qingdao, Shandong 266237*
[6] *Temple University, Philadelphia, Pennsylvania, 19122*
[7] *RIKEN Nishina Center for Accelerator-Based Science, Wako, Saitama 351-0198*
[8] *University of Illinois Urbana-Champaign, Urbana 61801*
[9] *Indiana University, Bloomington, Indiana 47408*

*The **RHIC Spin Collaboration** consists of the spin working groups of the RHIC collaborations, many theorists and members of the BNL accelerator department.

Contents

1 Executive Summary

RHIC has produced a remarkable breadth of physics results over the years, with compelling discoveries in both Hot and Cold QCD. It is critical to utilize the last two years of operations to complete the extraordinarily rich program that is uniquely possible with the $p+p$, p+A and A+A collisions provided by RHIC.

A significant piece of the RHIC legacy is the 25 years of innovation in accelerator science and experimental techniques necessary to collide highly polarized, high-energy proton beams. These achievements include the design and construction of the the world's highest intensity polarized proton source, the use of Siberian snakes to reduce the depolarizing effects of the resonance field harmonics, the implementation of spin rotators to provide proton beams polarized in the longitudinal, transverse or radial direction in the two primary interaction regions, and the development of techniques to maintain orbit and emittance stability from injection to full energy in order to maximize polarization lifetimes. In parallel, new techniques and tools were developed to monitor and evaluate the quality of the beams. As a result it is now possible to make precision measurements of the beam spin tune, to extract the transverse/radial polarization component in a longitudinally polarized beam and precisely measure the spin-dependent relative luminosities. These advances, along with the design, construction, and operation of absolute and relative high precision hadron polarimetry have played an essential role in the success of the RHIC experimental Cold QCD program and have laid the foundation for the design of the future Electron-Ion Collider's (EIC) highly polarized high energy light ion beams.

RHIC has driven the exploration of the fundamental structure of strongly interacting matter into new territory and will continue to enable advances in the field for years to come. These explorations have always thrived on the complementary nature of lepton scattering and hadronic probes. This is demonstrated clearly in the flagship measurements of the gluon and sea-quark helicity distributions that are discussed in Section 2. The sea-quark program exploited the advantages afforded by high energy hadron beams, using $W^{+/-}$ production to reveal the flavor asymmetry of the $\Delta\bar{u}$ and $\Delta\bar{d}$ distributions without the complications of fragmentation effects. Similarly, reconstructed jet and pion asymmetries were used for the first time to directly probe gluon interactions in proton-proton collisions, discovering a sizable gluon helicity distribution in the region $x > 0.05$, as shown in the left panel of Fig. 1.

The RHIC Cold QCD program leverages the techniques and tools developed in the high profile helicity program to open new frontiers in the rapidly evolving field of transverse spin physics. For example, the reconstruction of W bosons in transversely polarized proton collisions is used to test the predicted sign change of the Sivers' function and to provide the first constraints on the sea-quark Sivers functions. Hadron-in-jet asymmetries, measured for the first time at RHIC, and di-hadron asymmetries provide access to the collinear quark transversity distributions, as well as the transverse momentum dependent (TMD) Collins Fragmentation Function (hadron-in-jet) and collinear Interference Fragmentation Functions (di-hadron) in the final state. These new channels, and many more, are discussed in detail in Section 3. Again, the transverse spin program exploits the complementarity of the high energy hadron collider configuration by accessing distributions originally measured in lepton scattering experiments, but in a different kinematic regime, allowing for new insights into universality, factorization and TMD evolution.

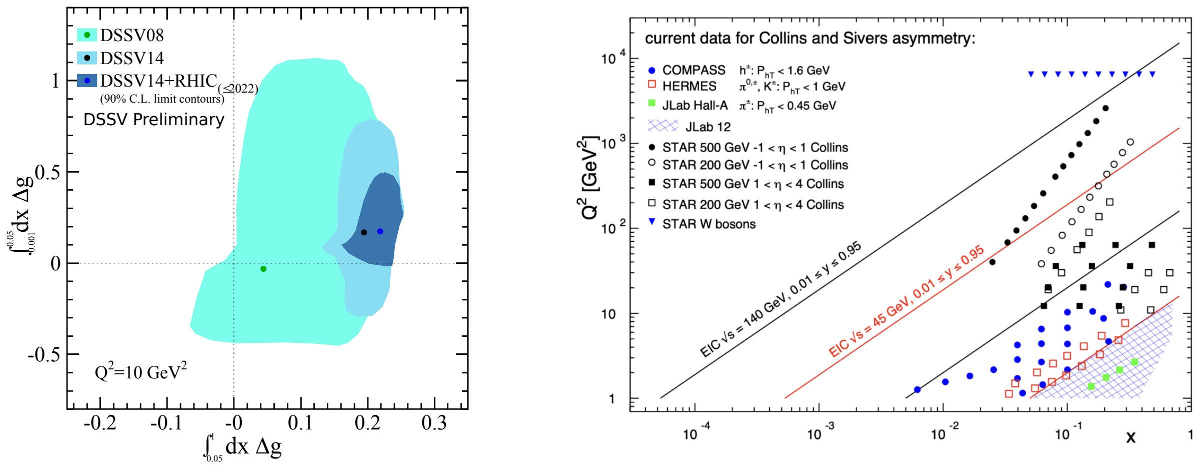

Figure 1: Left: The impact of RHIC data to constrain gluon helicity [1, 2]. Right: The x-Q^2 probed with data from the future EIC and Jlab-12 GeV as well as the current semi-inclusive deep inelastic scattering (SIDIS) data and the jet and W-boson data from RHIC. All data are sensitive to the Sivers function and transversity times the Collins fragmentation function (FF) in the TMD formalism.

As the realization of a future EIC draws closer, there is a growing scientific imperative to complete a set of "must-do" measurements in p+p and p+A collisions in the remaining RHIC runs. The ongoing RHIC Cold QCD program will build on the accelerator's unique ability to collide a variety of ion beams in addition to polarized protons, and a detector with wide kinematic coverage that has been further enhanced through an upgrade at forward rapidities consisting of electromagnetic and hadronic calorimetry as well as tracking. The new detectors will enable e/h discrimination with charge-sign determination and full jet reconstruction in the forward direction for the first time, allowing RHIC to extend the full complement of the existing transverse spin measurements into new kinematic regimes! This will expand the existing transverse spin program into both lower and higher x domains, as illustrated in the right panel of Fig. 1. In addition to the expanded transverse spin program, RHIC will be able to further explore exciting new signatures of gluon saturation and non-linear gluon dynamics (see Section 4). The ratios of forward Drell-Yan and photon-jet yields in p+p and p+A/A+A collisions are clean probes of nuclear modifications to initial state parton distributions as well as gluon saturation effects. All of these measurements rely critically on the successful completion of scheduled RHIC operations before the shutdown in 2025.

While the remaining RHIC Cold QCD program is unique and offers discovery potential on its own, successful completion of the RHIC program is also essential to fully realize the scientific promise of the EIC. These data will provide a comprehensive set of measurements in hadronic collisions that, when combined with EIC data, will establish the validity and limits of factorization and universality. The separation between the intrinsic properties of hadrons and interaction dependent dynamics, formalized by the concept of factorization, is a cornerstone of QCD and largely responsible for the predictive power of the theory in many contexts. While this concept and the associated notion of universality of the quantities that describe hadron structure has been successfully tested for unpolarized and - to a lesser extent - longitudinally polarized parton densities, its experimental validation remains an unfinished task for much of what the EIC is designed to study, namely the three-dimensional structure of the proton and the physics of dense partonic systems in heavy nuclei. To achieve these fundamental goals, it is essential to have data from both lepton-ion and proton-ion collisions, with an experimental accuracy that makes quantitative comparisons meaningful. The final experimental accuracy achieved with the data collected during this final RHIC campaign will enable quantitative tests of process dependence, factorization and universality by comparing lepton-proton with proton-proton collisions. When combined with data from the EIC, it will provide a broad foundation to a deeper understanding of Quantum Chromodynamics.

2 Collinear Proton Structure

- RHIC high precision longitudinally polarized proton-proton data for a variety of probes and center of mass energies have played a decisive role in constraining the sea-quark and gluon helicity distributions in the proton.

- W production in longitudinally polarized $p+p$ collisions revealed the existence of a flavor asymmetry in the polarization in the sea of light anti-quarks with $\Delta\bar{u}$ being positive, while $\Delta\bar{d}$ is negative.

- Collisions at center of mass energies of 200 GeV provided the first evidence that the gluons inside a proton are polarized. Data from the RHIC run in 2009, when included in global analyses, showed that gluons carry approximately 40% of the proton spin in the region where the gluon carries more than 5% of the proton momentum ($x > 0.05$) at $Q^2 = 10\,\text{GeV}^2$.

- The published and preliminary results based on data collected in 2012, 2013 and 2015 at center of mass energies of 200 and 510 GeV reduce the present uncertainties on gluon helicity Δg even further, providing more insights in the region of momentum fraction x between about 0.01 to 0.5 of the momentum of a polarized proton.

2.1 Achievements To-Date

2.1.1 W A_L and sea quark polarization

The STAR and PHENIX Collaborations have concluded the measurements of the parity-violating spin asymmetry in the production of weak bosons from collisions with one of the proton beams polarized longitudinally [3–8]. In 510 GeV center-of-mass proton-proton collisions at RHIC, W^+ bosons are produced primarily in the interactions of u quarks and $\bar{d}$ antiquarks, whereas W^- bosons originate from d quarks and $\bar{u}$ antiquarks. The longitudinal single spin-asymmetry (A_L) measurements of the decay positrons provide sensitivity to the u quark and $\bar{d}$ helicities in the proton, whereas the decay electrons do so for the d and $\bar{u}$ helicities. Combined, they make it possible to delineate the light quark and antiquark polarizations in the proton by flavor.

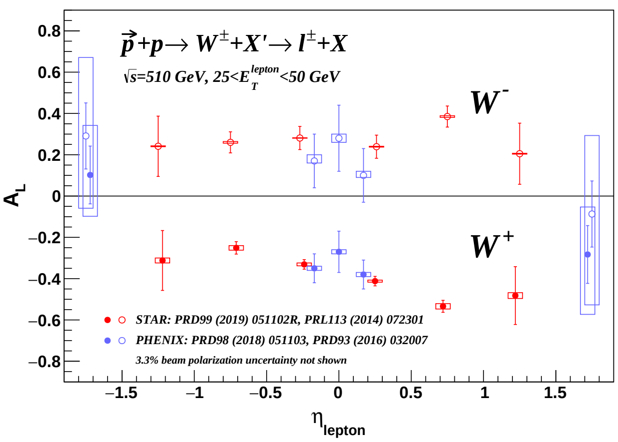

Figure 2: Longitudinal single-spin asymmetries, A_L, for W production as a function of the lepton pseudorapidity, η_{lepton}, for the combined STAR and PHENIX data samples [5–8].

These measurements shed light on understanding of the light quark polarizations − one of the two initial motivations for the spin-physics program at RHIC. The data, shown in Fig. 2, are the final results from STAR and PHENIX on this topic [5–8] that combine all the published data obtained in 2011, 2012, and 2013. The impact of the RHIC W data on the sea quark helicity distributions $\Delta\bar{u}$ and $\Delta\bar{d}$ is presented in Fig. 3. The plot shows the impact of the RHIC W data [5,6,8] from the new global fit by the DSSV group including also the recent jet, dijet, and pion data [11–17] (that constrain mostly the gluon helicity). The sea quark $\bar{u}$ helicity $\Delta\bar{u}$ is now known to be positive and $\Delta\bar{d}$ is negative. The STAR 2013 data [8] were also used in the reweighting procedure with the publicly available NNPDFpol1.1 PDFs [10]. The results from this reweighting, taking into account the total uncertainties of the STAR 2013 data and their correlations, are shown in Fig. 4 as the blue hatched bands. The NNPDFpol1.1 uncertainties are shown as the green bands for comparison. As seen from the plot, the data have now reached a level of precision that makes it possible, for the first time, to conclude that there is a clear asymmetry between the helicity distribution of $\bar{u}$ and $\bar{d}$, and it has the opposite sign from the $\bar{d}/\bar{u}$ flavor asymmetry in the unpolarized sea.

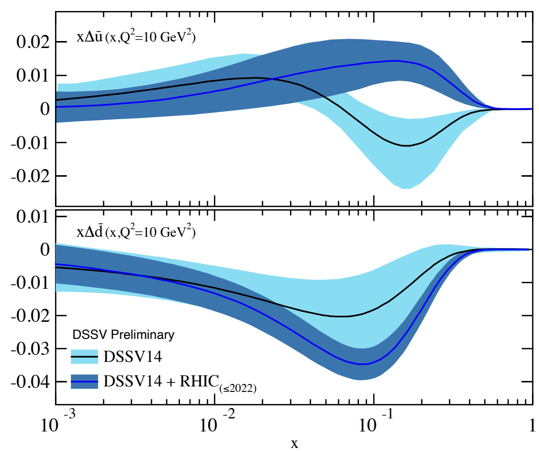

Figure 3: The impact of the RHIC W A_L results on $\bar{u}$ (top) and $\bar{d}$ (bottom) polarizations as a function of x at a scale of $Q^2 =$ 10 GeV^2. The black curves with the 1σ uncertainty bands marked in light blue show the results from the DSSV14 global fit [9] and the blue curves with 1σ uncertainty bands in dark blue show the results for the new preliminary DSSV fit [2] including the RHIC W data [5, 6, 8].

2.1.2 Double helicity asymmetries A_{LL} and gluon polarization

The measurement of the gluon polarization inside protons has been a major emphasis of the longitudinally polarized RHIC program. At RHIC, gluon polarization can be accessed by measurements of the spin-dependent rates of production of jets [12–14, 18–21], dijets [11–14, 22], π^0s and charged pions, [16, 17, 23–30], and direct photons [31]. Data from the RHIC run in 2009 have for the first time shown that gluons inside a proton are polarized with a strong constraint from the jet data at a center-of-mass energy of $\sqrt{s} = 200\,\text{GeV}$ [9, 10]. Perturbative QCD analyses [9, 10] of the world data, including 2009 inclusive jet and π^0 results, at next-to-leading order (NLO) precision, suggest that gluon spins contribute $\simeq 40\%$ to the spin of the proton for gluon fractional momenta $x > 0.05$ at a scale of $Q^2 = 10\,\text{GeV}^2$. Results for dijet production provide a better determination of the functional form of $\Delta g(x)$, compared to inclusive observables, because of better constraints on the underlying kinematics [32].

Recent STAR results [12–14] and preliminary results [15, 33] on longitudinal double-spin asymmetries of inclusive jet and dijet production at center-of-mass energies of 200 GeV (Run-15) and 510 GeV (Run-12 and Run-13) at mid and intermediate rapidity complement and improve the precision of previous STAR measurements. Figure 5 shows recent STAR results on inclusive jet A_{LL} versus $x_T = 2p_T/\sqrt{s}$ at $\sqrt{s} =$ 200 GeV and 510 GeV at mid-rapidity from data collected in years 2009-2015, and evaluations from the DSSV14 [9] and NNPDFpol1.1 [10] global analyses. The overall impact of the recent jet and dijet [11–15],

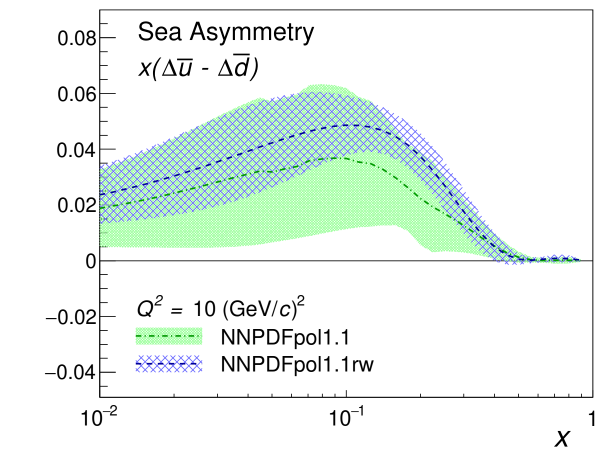

Figure 4: The difference of $\bar{u}$ and $\bar{d}$ polarizations as a function of x at a scale of Q^2= 10 GeV^2 before and after NNPDFpol1.1 [10] reweighting with STAR 2013 W A_L [8]. The green band shows the NNPDFpol1.1 results [10] and the blue hatched band shows the corresponding distribution after the STAR 2013 W data are included by reweighting.

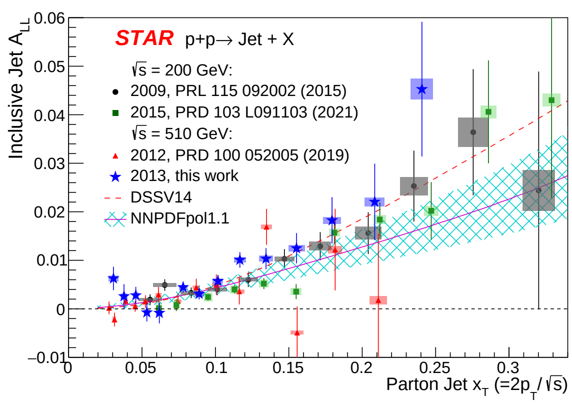

Figure 5: STAR results on inclusive jet A_{LL} versus x_T at $\sqrt{s}$ = 200 GeV [13, 21] and 510 GeV [12, 14] at mid-rapidity from data collected in years 2009-2015, and evaluations from DSSV14 [9] and NNPDFpol1.1 (with its uncertainty) [10] global analyses. The vertical lines are statistical uncertainties. The boxes show the size of the estimated systematic uncertainties. Scale uncertainties from polarization (not shown) are ±6.5%, ±6.6%, ±6.4% and ±6.1% from 2009 to 2015, respectively. Source: [14].

pion [16, 17] and W [6, 8] data on the x-dependence of the gluon helicity distribution at $Q^2 = 10\,\text{GeV}^2$ based on the global fit by the DSSV group is presented in Fig. 6. The truncated moment of the gluon helicity from the new DSSV evaluations [2] at $Q^2 = 10\,\text{GeV}^2$ integrated with the range of $x \in (0.001, 0.05)$ is 0.173(156) and in the range of $x \in (0.05, 1)$ is 0.218(27) (at 68% C.L.), which can be seen in the left panel of Fig. 1.

The truncated moment of the gluon helicity integrated from $x = 0.0071$ to 1 at $Q^2 = 10\,\text{GeV}^2$ from the recent JAM global QCD analysis [34] including a subset of RHIC data, i.e., STAR inclusive jet results, and assuming the SU(3) flavor symmetry and PDF positivity is 0.39(9). Authors of [34] also discuss the possibility of the solution with negative gluon contribution if the PDF positivity constraint is removed from the global fit. They argue that there is no fundamental theoretical requirement for PDF to be positive at all values of x, and therefore it would be highly desirable to have an observable which is linearly sensitive to gluon helicity distribution. Direct photons coming mainly from the quark-gluon Compton process and dijets narrowing down the parton kinematics are ideal probes to distinguish between positive and negative gluon helicity solutions. Figure 7 demonstrates the preference of positive solution with the PHENIX direct photon A_{LL} data [31]. Figure 8 shows that the STAR dijet data [14] also strongly disfavors distributions with large and negative gluon helicities.

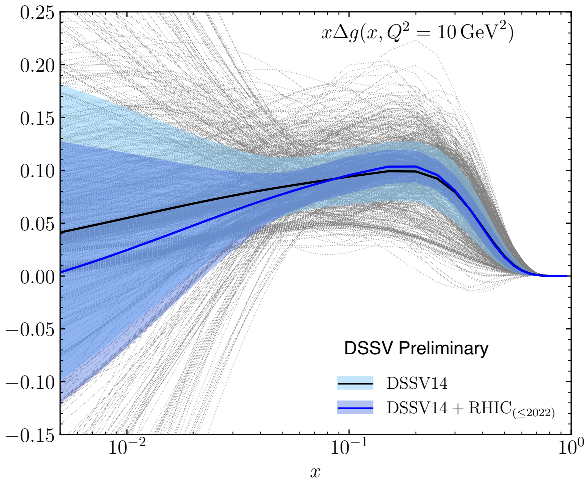

Figure 6: The impact of the recent jet and dijet [11–15], pion [16, 17] and W [5, 6, 8] data on the x-dependence of the gluon helicity distribution at $Q^2 = 10\,\mathrm{GeV}^2$ based on the global fit by the DSSV group. The black curve with the 1σ uncertainty light blue band illustrates the DSSV14 results [9], while the blue curve with 1σ uncertainty band in dark blue [2] shows the preliminary results after the inclusion of the new data.

In the plot the asymmetries A_{LL} are presented for four dijet event topologies, namely, with forward-forward jets (top left), forward-central jets (top right), central-central jets (bottom left), and forward-backward jets (bottom right), where forward jet rapidity is $0.3 < \eta < 0.9$, central jet rapidity is $|\eta| < 0.3$, and backward jet rapidity is $-0.9 < \eta < -0.3$. The forward-forward and forward-central configurations probe the most asymmetric collisions down to $x \simeq 0.015$. The forward-forward and central-central events probe collisions with $|\cos\theta^*|$ near zero, whereas forward-central and forward-backward events are more sensitive to larger $|\cos\theta^*|$, where θ^* is the scattering angle in the center-of-mass frame of scattering partons. In both Figs. 7 and 8, the DSSV14 calculations are plotted as the black curves with the 1σ uncertainty bands marked in light blue. The blue curves with 1σ uncertainty bands in dark blue show the impact of all the data sets included in the new preliminary DSSV fit [2] as in Fig. 6. The curves for JAM $\Delta g < 0$ solution [34] are presented in red.

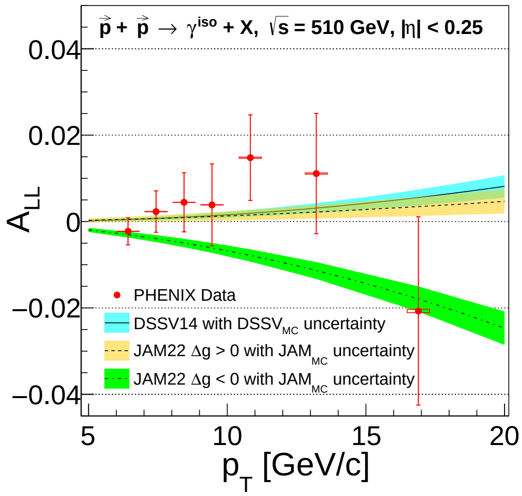

Figure 7: PHENIX double-helicity asymmetry A_{LL} vs p_T for isolated direct-photon production in polarized p+p collisions at $\sqrt{s}$=510 GeV at midrapidity [31]. The DSSV14 and JAM22 calculations are shown with 1σ uncertainty band obtained from MC replicas (see references in [31]).

2.2 Future Opportunities

2.2.1 PHENIX

A few more PHENIX analyses are ongoing and are expected to be accomplished and published. They are based on the largest data set from longitudinally polarized proton collisions collected in Run-2013, and will conclude the longitudinal spin program with PHENIX:

- A_{LL} for clusters in forward EM calorimeter MPC ($3.1 < |\eta| < 3.9$) at $\sqrt{s}$=510 GeV, which are mainly contributed by π^0s. Such data will significantly extend the kinematic reach in x towards values of a few times 10^{-3} where the gluon helicity is unconstrained so far. The MPC was equipped with new electronics before Run-2013, and therefore requires additional efforts for calorimeter calibration. The analysis is steadily progressing.

- Cross section and A_{LL} in η-meson production at mid-rapidity. The cross section measurement is expected to give a significant input for the extraction of η fragmentation functions (as did our previously published data at $\sqrt{s}$=200 GeV [35]) which are still only poorly known. The A_{LL} data will add to the constraint of $\Delta g(x)$. The analysis is planned to be done by the University of Michigan group.

2.2.2 STAR

As discussed in section 2.1.2, measurements of the longitudinal double-spin asymmetry A_{LL} have provided increasing tight constraints on the helicity preferences of gluons within the proton, especially for those gluons carrying at least 5% of the proton's momentum. Constraints on gluons of lower momentum fraction, however, remain weak, as can be seen by projecting the left plot shown in Fig. 1 onto the vertical axis. The truncated moment of

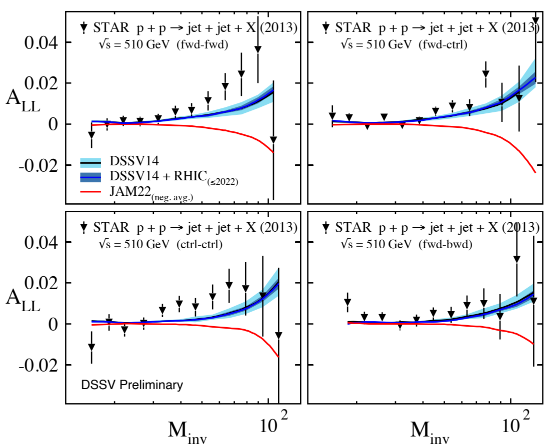

Figure 8: STAR double-helicity asymmetries A_{LL} for dijet production vs dijet invariant mass M_{inv} in polarized $p+p$ collisions at $\sqrt{s}$=510 GeV at midrapidity from 2013 data set [14]. DSSV14 evaluation [9] is plotted as the black curve with the 1σ uncertainty band marked in light blue. The blue curve with 1σ uncertainty band in dark blue shows the impact of all the data sets included in the new preliminary DSSV fit [2] as in Fig. 6. The red curves show the JAM $\Delta g < 0$ solution [34] calculated by the DSSV group.

$\Delta g(x)$ over the range $x \in (0.001, 0.05)$ is 0.173 with an uncertainty ($1\ \sigma$) of 0.156, a result consistent both with zero and with a 60% contribution to the proton spin.

To address this, over the next year STAR will be completing analyses that focus specifically on measurements of polarized asymmetries in kinematic regimes, and using experimental techniques, that will provide much tighter constraints on the gluon helicity distribution at low momentum fraction, $x < 0.1$. To extract the asymmetries most relevant for this regime, where gluons are abundant and the shape of $\Delta g(x)$ is constrained primarily just by its assumed functional form, we pushed our measurement program in several directions. By detecting jets at more forward rapidities (larger η) and higher center-of-mass energies (larger $\sqrt{s}$), we collect data sets dominated by hard scatterings of high-x (valence, highly polarized) quarks on the low-x gluons of primary interest. By focusing on dijet events, and triggering on jets with a low-p_T jet in coincidence, the collected data samples can be more directly sorted based on the momentum fractions x_1 and x_2 carried by the initial-state partons [22], with enhanced statistics at low x_2.

Preliminary results from STAR for the double-spin asymmetry A_{LL} for dijet production at intermediate pseudorapidities are shown in Fig. 9 for $p+p$ collision data taken at $\sqrt{s}$ = 200 GeV in 2015 and at 510 GeV in 2012 and 2013. Results are plotted as a function of the dijet invariant mass M divided by the collision energy.

These new data are generally consistent, and thus support, current global analyses that have incorporated previous RHIC results. Of particular interest is the bottom plot, which

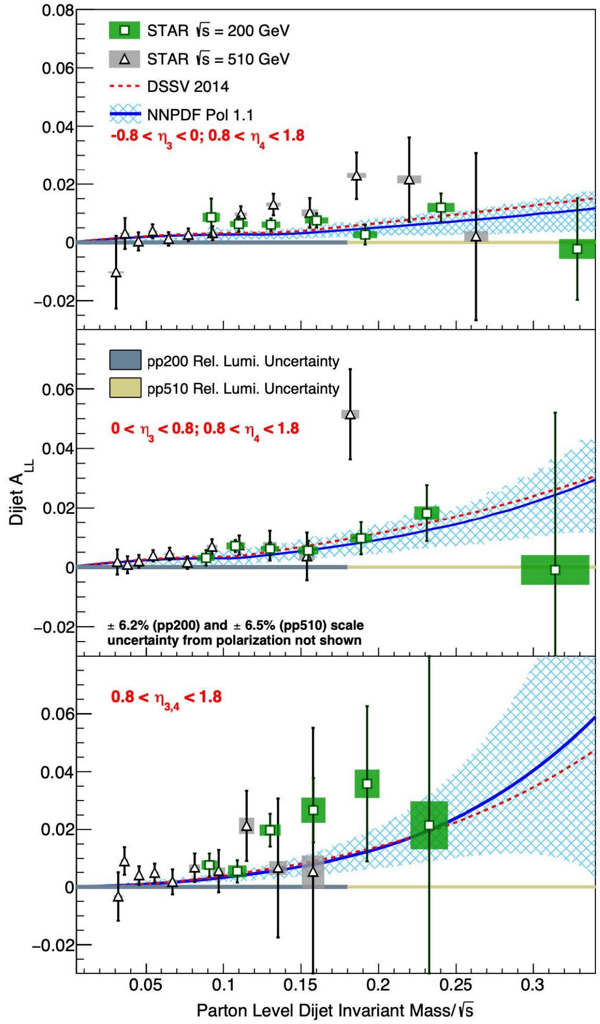

Figure 9: A_{LL} as a function of $M_{inv}/\sqrt{s}$ for dijets measured in 2012 and 2013 at $\sqrt{s}$ = 510 GeV compared to STAR data from 2015 at 200 GeV. Results are shown for the East Barrel-Endcap (top), West Barrel-Endcap (middle), and Endcap-Endcap (bottom) topologies.

shows the asymmetries measured when both jets are detected in the STAR Endcap. These "forward-forward" jet pairs arise from the collisions that, in a collinear $2 \to 2$ framework, are most kinematically asymmetric at the parton level, $x_1 \gg x_2$, which are dominated by quark-gluon scattering at RHIC energies. In the low-mass region on this plot, where simulations indicate that $x_2 \approx x_g \in (0.006, 0.03)$, the data taken at $\sqrt{s} = 510$ GeV are seen to lie above predictions, suggesting non-zero contributions to $\Delta g(x)$ from these low-x gluons.

The STAR Collaboration is also finalizing precise cross section measurements for inclusive jet production in p+p collisions at $\sqrt{s} = 200$ and 510 GeV. Differential cross sections are being extracted as functions of the jet transverse momentum p_T and jet pseudorapidity η at each energy, with corrections for underlying event contributions estimated using an off-axis cone technique. These inclusive jet cross sections are expected to further constrain the gluon parton distribution function in the proton, can be used to tune Monte Carlo event generators, and will provide critical reference data needed to study the quark-gluon plasma at STAR.

3 Three-dimensional Structure

STAR and PHENIX opened new territory in studying the 3D structure of the proton in the region of momentum fractions down to $x \sim 0.01$ and high Q^2, a region not probed by prior experiments. See Fig. 10.

- The collected unique sets of transversely polarized data in p+p and p+A collisions, including the most recent campaign with the forward upgrade, will be finalized with the 2024 RHIC run by STAR and sPHENIX.
- To accomplish the scientific mission of the transverse spin program, it is imperative that analysis activities continue to be supported throughout the upcoming years. These activities offer discovery potential of their own, and they are critical for properly interpreting data from the future Electron-Ion Collider.
- STAR pioneered the novel use of jets and their substructure to study initial and final state transverse momentum dependent (TMD) effects in polarized p+p collisions. For example, the measured single-spin asymmetries of identified hadrons in jets probe the quark transversity distribution and Collins TMD fragmentation function, and the single-spin asymmetry of dijet opening angle is sensitive to the Sivers TMD parton distribution. The large rate capabilities of sPHENIX will augment these measurements to higher jet transverse momenta for charged hadrons within the jet.
- STAR has also measured quark transversities via dihadron interference fragmentation functions. The results from early measurements have been included in a global analysis, and found to provide significant constraints. Ongoing analysis of more recent STAR data, together with the data that STAR will record during 2024, will provide far more stringent constraints. Also here sPHENIX will be able to provide additional measurements using charged hadrons.

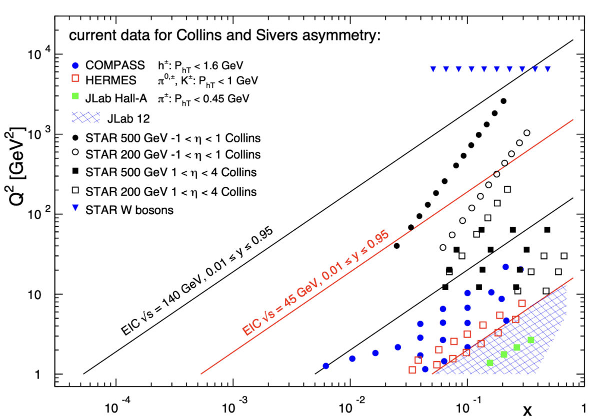

Figure 10: The x-Q^2 probed with data from the future EIC and Jlab-12 GeV as well as the current SIDIS data and the jet and W-boson data from RHIC. All data are sensitive to the Sivers function and transversity times the Collins FF in the TMD formalism.

- Substantial progress on the large forward transverse single-spin asymmetry puzzle has been made. The A_N of the isolated π^0s was found to be significantly larger than that for non-isolated ones both in p+p and p+A collisions at STAR. The A_N for π^0s at large x_F, far forward pseudorapidity ($\eta > 6$), and $p_T < 1$ GeV/c at RHICf was found to be comparable to that at the same x_F, but with $2.5 < \eta < 4$ and $p_T > 2$ GeV/c at STAR. The A_N for electromagnetic jets was found to be small but non-zero, which provided significant constraints to the quark Sivers function. The A_N for forward diffractive EM-jets has been measured and found not to be the source of the large A_N. In fact, it favors a negative contribution.

- Transverse single-spin asymmetry A_N of weak bosons, sensitive to the Sivers TMD function, has been probed at STAR. With the increased precision provided by 2017 data, STAR found smaller asymmetries than were suggested by 2011 data. As a result, the increased statistics of the 2022 dataset are critical to improve the precision of our asymmetry measurements in order to provide a conclusive test of the Sivers' function sign change.

- PHENIX has measured transverse single-spin asymmetries at mid-rapidity that provide constraints on the twist-3 correlation functions of quarks and gluons, including the first RHIC result of direct photon A_N, open heavy flavor decay electron A_N, and high precision neutral meson A_N.

- sPHENIX with its capabilities to record data at high rates and reconstruct jets and decays of heavy-flavor hadrons will in some channels significantly improve the precision of transverse single-spin asymmetries at mid-rapidity in particular as compared to PHENIX.

- PHENIX and STAR have both measured the nuclear dependence of the forward inclusive hadron single-spin asymmetries. PHENIX finds a strong nuclear dependence for positive hadrons at $1.2 < \eta < 2.4$, whereas STAR finds a weak nuclear dependence for π^0 at $2.7 < \eta < 3.8$. Neither the origin of the nuclear dependence, nor the difference between the PHENIX and STAR results is well understood at this time.

- Transverse single-spin asymmetry of exclusive J/ψ photoproduction in ultra-peripheral collisions is expected to directly probe the generalized parton density (GPD) distribution. The STAR forward detector and data beyond 2022 can measure unique kinematic phase space, e.g., close to the threshold production energy of J/ψ, where a large asymmetry signal is expected.

3.1 Achievements To-Date

3.1.1 Studies of initial and final state TMD effects with jets

STAR has pioneered the novel use of jets and their substructure to study initial state and final state TMD effects in polarized $p+p$ collisions.

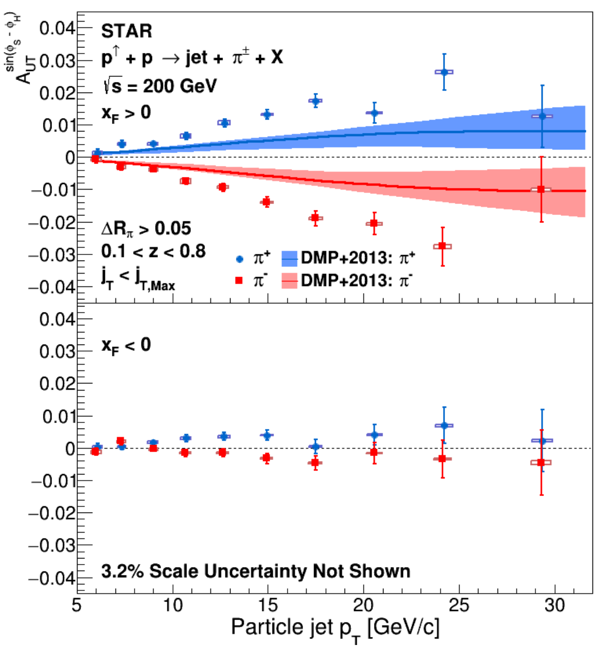

Figure 11: Collins asymmetry plotted for identified π^+ (blue) and π^- (red) particles as a function of jet p_T for jets that scatter forward relative to the polarized beam ($x_F > 0$) in the top panel and those that scatter backward ($x_F < 0$) in the lower panel, extracted from data collected in 2012 and 2015 [36]. The full ranges of both z and j_T are integrated over. Theoretical evaluations from [37] with their uncertainties are presented for π^+ (blue) and π^- (red). Source: [36].

The single-spin asymmetries of the azimuthal distribution of identified pions, kaons, and protons in high-energy jets measured at STAR probe the *collinear* quark transversity in the proton, coupled to the transverse momentum dependent Collins fragmentation function [38–40]. This makes $p+p$ collisions a more direct probe of the Collins fragmentation function than SIDIS, where a convolution with the TMD transversity distribution enters. The Collins asymmetry in $p+p$ collisions is an ideal tool to explore the fundamental QCD questions of TMD factorization, universality, and evolution. Figure 11 shows the recent results on combined 2012 and 2015 Collins asymmetries for charged pions within jets as a function of jet p_T [36]. By integrating over the hadron longitudinal and transverse momenta within the jets, Fig. 11 is sensitive primarily to the quark transversity. The measured asymmetries for jets that scatter forward relative to the polarized beam are larger than theoretical predictions [37], which are based on the transversity and Collins fragmentation function from SIDIS and e^+e^- processes within the TMD approach. Alternatively, the asymmetries can be investigated as functions of z, the fraction of jet momentum carried by the hadron, and j_T, the momentum of the pion transverse to the jet axis, as shown in Fig. 12. This provides a direct measurement of the kinematic dependence of the Collins fragmentation function. The j_T dependence appears to vary with z, contrary to the assumptions of most current phenomenological models [38–40]. STAR has also published Collins asymmetry measurements from a smaller 500 GeV data set collected in 2011 [41]. While statistics are limited, the results are consistent with those at 200 GeV for overlapping x_T, despite sampling Q^2 that is larger by a factor of 6. Analysis of the higher statistics 510 GeV data collected in 2017 is underway and will provide unique insight into the Q^2 evolution of the Collins TMD fragmentation function. Concurrent with the Collins effect measurements, STAR has also measured azimuthal modulations that are sensitive to the twist-3 analogs of the quark and gluon Sivers functions and to linear polarization of gluons in transversely polarized protons [36, 41]. Analysis is also underway to determine the unpolarized TMD fragmentation functions.

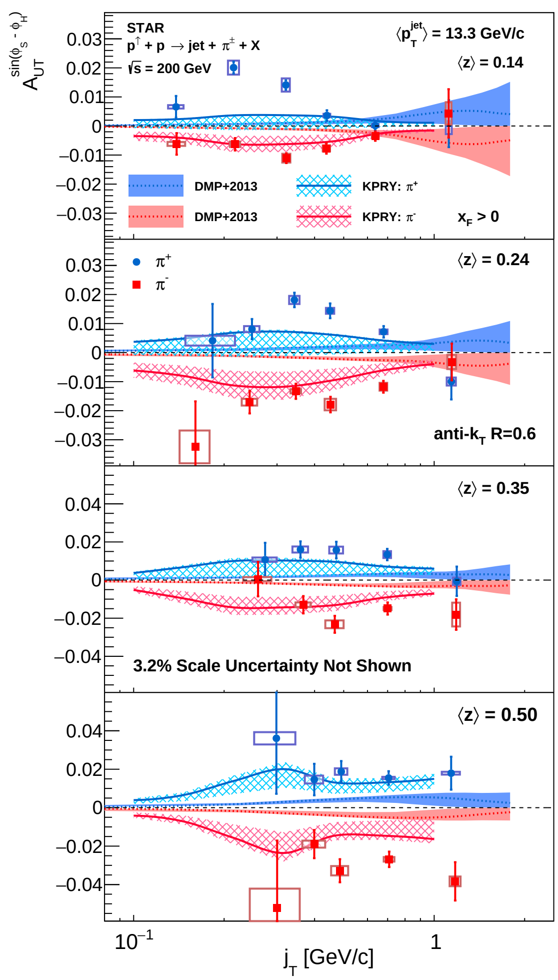

Figure 12: Collins asymmetry plotted for identified π^+ (blue) and π^- (red) particles as a function of j_T for four separate bins of hadron z, in jets with $p_T > 9.9$ GeV/c and $0 < \eta < 0.9$. Theoretical evaluations from [39] and [37] are also shown. Source: [36].

Another example of utilizing jets to unravel the internal TMD structure of the proton is the measurement of the asymmetry of the spin-dependent 'tilt' of the dijet opening angle, which is sensitive to the Sivers TMD PDF. For transversely polarized protons, the Sivers effect probes whether the transverse momentum $\vec{k}_T$ of the constituent quarks is preferentially

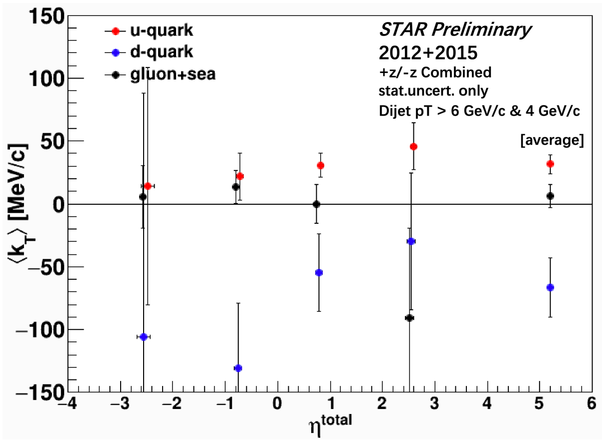

Figure 13: Preliminary results of the average transverse momentum $\langle k_T \rangle$ for individual partons, inverted using parton fractions from simulation and tagged $\langle k_T \rangle$ in data, plotted as a function of summed pseudorapidities of the outgoing jets $\eta_{\text{total}} \sim \log(x_1/x_2)$. (Positive η_{total} represents dijets emitted in the direction of the polarized beam.) The rightmost points represent the average of all the η_{total} bins. The systematic uncertainty in η_{total} is set to be non-zero to improve the visibility of the error bars. Source: [42].

oriented in a direction perpendicular to both the proton momentum and its spin. Figure 13 shows the first-ever observation of the Sivers effect in dijet production from the 200 GeV transverse spin data that STAR recorded in 2012 and 2015 [42]. The jets are sorted according to their net charge Q, yielding jet samples with enhanced contributions from u quarks (positive Q) and d quarks (negative Q), with a large set near $Q = 0$ dominated by gluons. Simple kinematics allow for conversion from the spin-dependent 'tilt' of the dijet pair to a value of k_T on an event-by-event basis. Finally, the results are unfolded for the k_T of individual partons. Such measurements are crucial to explore questions regarding factorization of the Sivers function in dijet hadroproduction [43–46]. New data to be taken in 2024 will reduce the uncertainties for the region of summed pseudorapidities of the outgoing jets $|\eta_3 + \eta_4| < 1$ by about a factor of two. The increased acceptance from the iTPC will reduce the uncertainties at $|\eta_3 + \eta_4| \approx 2.5$ by a much larger factor, while the Forward Upgrade will enable the measurements to be extended to even larger values of $|\eta_3 + \eta_4|$. When combined with the 510 GeV data from Run-17 and Run-22, the results will provide a detailed mapping *vs.* x for comparison to results for Sivers functions extracted from SIDIS, Drell-Yan, and vector boson production.

3.1.2 Transversity from di-hadron interference fragmentation functions

STAR has also measured quark transversity via dihadron Interference Fragmentation Functions (IFF) in 200 and 500 GeV p+p collisions [47, 48], as shown in Fig. 14. The IFF is a collinear observable, so these measurements provide a complementary probe of transversity relative to the Collins asymmetry measurements that obeys different evolution equations. The results from the first measurements at 200 GeV, which were based on data recorded during 2006 [47], have been included together with IFF measurements from SIDIS in a global analysis [49] that is also shown in Fig. 14. The STAR IFF measurements were found to provide significant additional constraints on the u- and d-quark transversities. The dominant systematic uncertainties in the global analysis arose from the current lack of knowledge regarding the unpolarized gluon dihadron fragmentation functions.

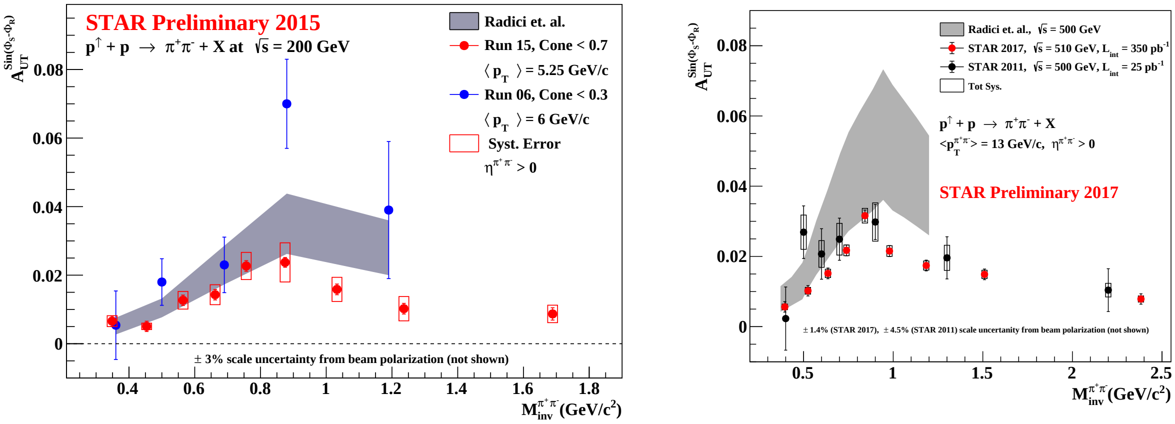

Figure 14: A comparison of STAR published [47, 48] and preliminary IFF asymmetries vs. dipion invariant mass to predictions from the global analysis [49] for 200 GeV (left) and for 500/510 GeV (right). The p_T bins at 200 and 500/510 GeV have been chosen to sample similar values of $x_T = 2p_T/\sqrt{s}$.

3.1.3 Transverse single-spin asymmetry in the forward region

RHIC measurements have demonstrated the persistence of sizeable transverse single-spin asymmetries A_N for forward π^0 production at RHIC energies up to 510 GeV with a weak energy dependence (see left panel of Fig. 15), where different QCD mechanisms including higher twist effects, TMD effects like the Sivers or Collins effects, and diffractive processes could all contribute. It is thus important to study different effects separately for a full understanding of the underlying mechanism, and a series of measurements were performed in p+p collsions at both 200 and 500 GeV and in p+A collisions at STAR [50–52].

Firstly, the topological dependence of the π^0 A_N was studied, and the A_N of the isolated π^0's (meaning no other particles around) are significantly larger than the non-isolated ones,

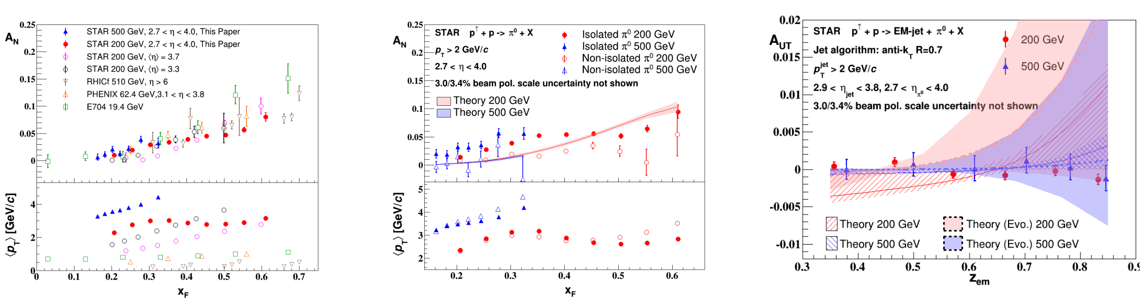

Figure 15: Left: Transverse single-spin asymmetry A_N as a function of x_F for inclusive π^0 in p+p collisions up to RHIC energies of 200 and 510 GeV. Middle: A_N asymmetries for the isolated and non-isolated π^0 in p+p collisions at 200 and 500 GeV. Right: The Collins asymmetry for π^0 in an electromagnetic jet for p+p collisions at $\sqrt{s}$ = 200 and 500 GeV. The plots are from [50].

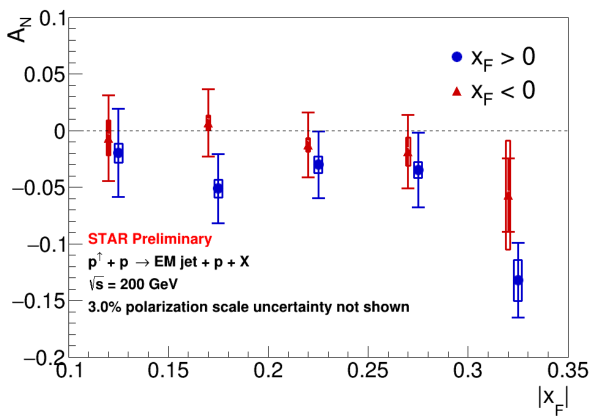

Figure 16: Transverse single-spin asymmetry for diffractive EM-jet as a function of x_F in transversely polarized proton-proton collisions at $\sqrt{s} =$ 200 GeV [52]. The blue points are for $x_F > 0$. The red points are for $x_F < 0$ with a constant shift of -0.005 along x-axis for clarity. The rightmost points are for $0.3 < |x_F| < 0.45$.

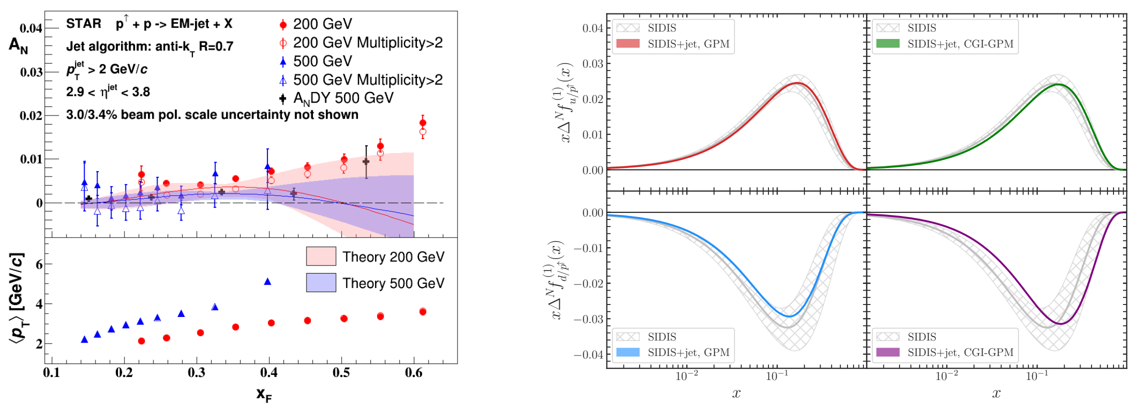

Figure 17: Left: Transverse single-spin asymmetry as a function of x_F for electromagnetic jets in transversely polarized proton-proton collisions at $\sqrt{s} =$ 200 and 500 GeV [50]. Right: Comparison between the Sivers first $k_\perp$-moments from SIDIS data and their reweighted SIDIS+jet (data from STAR) in two frameworks: GPM and CGI-GPM [53].

as shown in the middle panel of Fig. 15. Consistent results were obtained in both p+p and p+A collisions with very weak A dependence in p+A [50, 51]. This triggered discussions on the possible contribution from the diffractive process, which motivated a measurement of A_N for singly and double diffractive events, utilizing the STAR Roman Pot detectors to tag diffractive processes with scattered protons close to the beamline. Figure 16 shows the preliminary results for forward diffractive EM-jet A_N as a function of x_F at $\sqrt{s} =$ 200 GeV [52]. The results favor a non-zero negative A_N with 3.3 σ significance, so these diffractive processes are most probably not the source of the large positive A_N of π^0. The negative contribution from diffractive jets is not currently described by theory.

In studying the contribution from the final-state effect, STAR also measured the Collins asymmetry of π^0 in an electromagnetic jet, which is shown in the right panel of Fig. 15. The measured Collins asymmetry was consistent with zero, in agreement with a theoretical

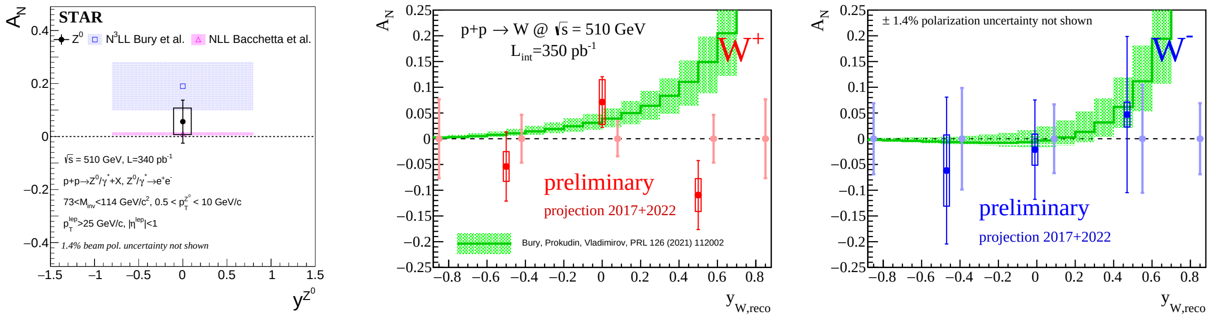

Figure 18: Left: Transverse single-spin asymmetry of Z^0 from STAR 2017 data [56]. The results are compared with the calculation from [57]. Middle and Right: Transverse single-spin asymmetry of $W^\pm$ from STAR 2017, and the projected statistical uncertainties from 2017 and 2022 data. The results are compared with calculation from [57] based on the next-to-next-to-next-to leading log ($\mathrm{N^3LL}$) accuracy TMD evolution from [58].

prediction based on collinear twist-3 factorization, resulting from significant cancellation between Collins effects of different quark flavors [39].

In a closely related study, RHICf has measured A_N for neutral pions in 510 GeV p+p collisions at very large pseudorapidity ($\eta > 6$), very large x_F (up to 0.8), and $p_T < 1$ GeV/c [54]. The asymmetries that they found are similar to those at comparable x_F and much higher p_T, as shown in the left panel of Fig. 15. A very recent calculation [55] based on diffractive triple Regge exchange provides a very good description of the RHICf A_N results.

Another study is the measurement of the A_N for inclusive electromagnetic jets, which is considered only related to the initial-state effect. The results of electromagnetic jet A_N in both 200 and 500 GeV p+p collisions are shown in the left panel of Fig. 17. The electromagnetic jet A_N was found to increase with x_F, but the magnitude is much smaller than the π^0 A_N. These data have been included in the recent global fit of the Sivers function [53], and showed a significant impact in constraining the Sivers function, as shown in the right panel of Fig. 17.

3.1.4 Transverse single-spin asymmetry of weak bosons

Proton-proton collisions at $\sqrt{s} = 510$ GeV allow STAR to study the evolution and sign change of the Sivers function with weak bosons at mid-rapidity ($-1 < y^{W^\pm/Z^0} < 1$). By focusing on interactions in which the final state involves only leptons, and hence the transverse partonic motion must be in the initial state, one can test the predicted sign change in A_N relative to interactions in which these terms must appear in the final state, such as SIDIS measurements. Following the low statistics proof-of-principle measurement using the 2011 data, STAR measured the transverse single-spin asymmetry A_N for W and Z with 2017 data, which had about 14 times more integrated luminosity.

In Fig. 18, the recent preliminary results on A_N of W and the publiahed results on A_N of Z^0 [56] are compared with predictions from [57, 58] that include STAR 2011 data. The

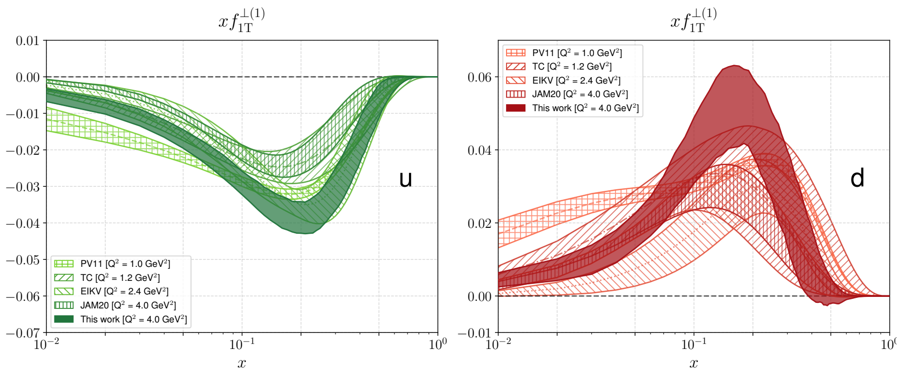

Figure 19: The first transverse moment $xf_{1T}^{\perp(1)}$ of the Sivers TMD as a function of x for the up (left panel) and down quark (right panel) extracted from world data including STAR 2011 W/Z data. Solid band: the 68% confidence interval obtained in this work at $Q^2 = 4$ GeV^2. The plot is from [59].

recent global QCD extraction of the Sivers function including STAR 2011 W and Z A_N data from [59] can be found in Fig. 19. With the increased precision provided by Run-17, we find smaller asymmetries than were suggested by Run-11. As a result, the increased statistics of the 2022 dataset are critical to improve the precision of our asymmetry measurements in order to provide a conclusive test of the Sivers' function sign change. Projected statistical uncertainties of W A_N from combined 2017 and 2022 data can be found in Fig. 18. The figure also illustrates that the improved tracking capabilities provided by the STAR iTPC upgrade will allow us to push our mid-rapidity $W^{\pm}$ and Z measurements to larger rapidity $y^{W/Z}$, a regime where the asymmetries are expected to increase in magnitude and the anti-quark Sivers' functions remain largely unconstrained.

3.1.5 Transverse single-spin asymmetries of direct photons and heavy flavor decay leptons

PHENIX has reported the first direct photon transverse single-spin asymmetry result at RHIC [60]. The asymmetry was measured at midrapidity $|\eta| < 0.35$ in p+p collisions at $\sqrt{s} = 200$ GeV. Photons do not interact via the strong force, and at this kinematics they are produced dominantly by the quark-gluon Compton process. Therefore, the measurement offers a clean probe of gluon dynamics that is only sensitive to initial-state effects. The asymmetry is shown in Fig. 20 and is consistent with zero to within 1% across the measured p_T range. The result is also compared with predictions from collinear twist-3 correlation functions. The solid green curve shows the contribution from qgq correlation function [61] while the dashed (blue) and dotted (red) curves are from ggg correlation functions [62]. Given the small predicted contributions from qgq correlation functions to the asymmetry, the result can provide a constraint on the ggg correlation function. sPHENIX is expected to significantly improve direct photon A_N measurements shrinking the uncertainties by more than a factor of two.

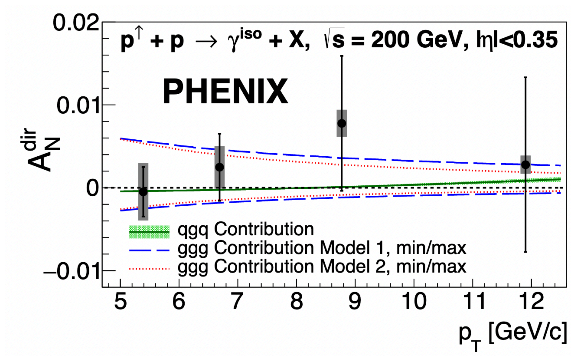

Figure 20: Transverse single-spin asymmetry of isolated direct photons at $\sqrt{s} = 200$ GeV compared with calculations from qgq and ggg correlation functions. Source: [60].

Similarly, the production of open heavy flavor at RHIC energies is dominated by gluon-gluon hard interactions. As such, also in single-spin asymmetries of heavy flavor decay leptons no final-state effect contributions are expected, and one is almost entirely sensitive to the initial state effects of the gluon correlators. The recent heavy flavor decay electron single-spin asymmetries at central rapidities obtained at PHENIX [63] are the first that quantify the gluon correlator contributions in two theoretical models [64, 65], as can be seen in Fig. 21. While each decay lepton asymmetry is only sensitive to a linear combination of the two model parameters, the combination of both charges enables the determination of both. In the 2024 data taking period, these measurements can be augmented by sPHENIX measurements that reconstruct D mesons directly and are expected to provide even higher precision to the tri-gluon correlator.

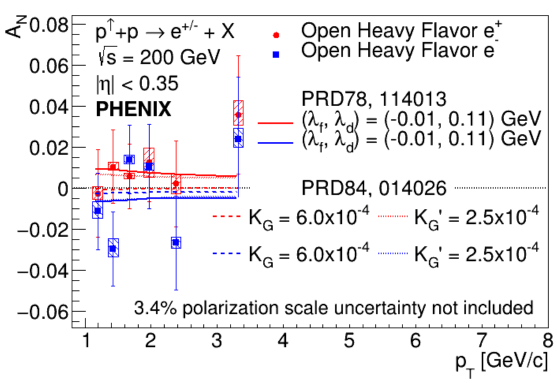

Figure 21: Transverse single-spin asymmetries of heavy flavor decay electrons at $\sqrt{s} = 200$ GeV [63] including parameterizations of the tri-gluon correlator in two theoretical models and the best values fitting the data [64, 65].

3.2 Future Results

3.2.1 PHENIX

A few more PHENIX analyses are ongoing and are expected to be accomplished and published:

- A_N of muons from open heavy flavor decays. The analysis is based on the largest data set from transversely polarized proton beam collisions at $\sqrt{s}$=200 GeV collected in Run-2015, and is expected to significantly improve PHENIX previously published data for muon A_N. The analysis is in an advanced stage and will give a significant constraint on the Twist-3 tri-gluon correlation function.

- A_N of forward η-meson production in forward EM calorimeter MPC ($3.1 < |\eta| < 3.9$) at $\sqrt{s}$=200 GeV, collected in Run-2012. It will improve the earlier PHENIX published results. The analysis is in the final stage, and will help to understand the nature of large A_N in forward region through the mass or isospin dependence.

3.2.2 STAR

As shown in Fig. 10, data from 200 GeV $p+p$ collisions from the upcoming run 2024 with the STAR Forward Upgrade will interpolate between the coverage that we will achieve with the forward data collected at 510 GeV in 2022 at high-x and the data at low-x from the STAR mid-rapidity detectors. Overall, all STAR data will provide valuable information about evolution effects and, with the projected statistical precision presented in Fig. 22, will establish the most precise benchmark for future comparisons to ep data from the EIC. It is also important to recognize that the hadron-in-jet measurements with the STAR Forward Upgrade will provide a very valuable experience detecting jets close to beam rapidity that will inform the planning for future jet measurements in similar kinematics at the EIC.

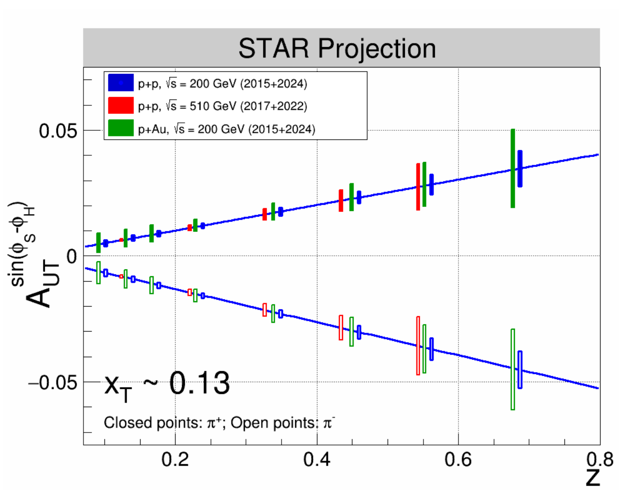

Figure 22: Projected statistical uncertainties for STAR Collins asymmetry measurements at $0 < \eta < 0.9$ in $p+p$ at $\sqrt{s}$ = 200 and 510 GeV and $p+$Au at $\sqrt{s_{\rm NN}}$ = 200 GeV. The points have arbitrarily been drawn on the solid lines, which represent simple linear fits to the STAR preliminary 200 GeV $p+p$ Collins asymmetry measurements from 2015. (Note that only one bin is shown spanning $0.1 < z < 0.2$ for 510 GeV $p+p$, whereas three bins are shown covering the same z range for the 200 GeV measurements.)

STAR also has the unique opportunity to extend the Collins effect measurements to nuclei. This will provide an alternative look at the universality of the Collins effect in hadron production (by dramatically increasing the color flow options of the sort that have been predicted to break factorization for TMD PDFs like the Sivers effect [43,44]) and explore the spin dependence of the hadronization process in cold nuclear matter. STAR collected a proof-of-principle dataset during the 2015 pAu run that is currently under analysis. Those data will provide the first estimate of medium-induced effects. However, the small nuclear effects seen by STAR for forward inclusive π^0 A_N [51] indicate that greater precision will likely be needed. Figure 22 shows the projected statistical uncertainties for the pAu Collins asymmetry measurement at $\sqrt{s_{\rm NN}} = 200$ GeV from 2015 and 2024 data, compared to those for p+p at the same energy.

An alternative way to look at the hadronization process in jets is to measure correlation functions of the energies of final state hadrons within a jet [66] [67]. The energy flow operator is defined as $\epsilon(\vec{\eta}) = \int_0^\infty dt \lim_{r\to\infty} r^2 n^i T_{0i}(t, r\vec{\eta})$ where $\vec{n}$ is a unit vector pointing in the direction of the energy flow and T_{0i} is the energy momentum tensor. The correlation function $< \epsilon(\vec{\eta_1})\epsilon(\vec{\eta_2})\ldots\epsilon(\vec{\eta_n}) >$ of the energy flow operators characterize the relationship between the energy of particles within a jet and their angular separation (R_L) from other particles.

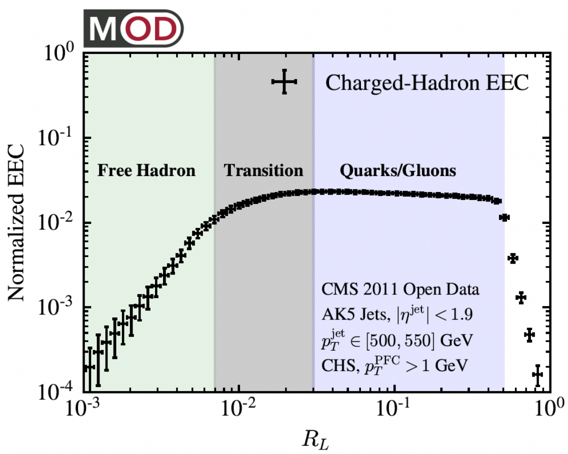

Figure 23: Two point EEC of charged hadrons in jets from Run 11 CMS open data [68].

$$EEC_{norm} = \frac{1}{\Sigma_{jets}\Sigma_{i\neq j}\frac{E_iE_j}{p^2_{T,jet}}} \frac{d(\Sigma_{jets}\Sigma_{i\neq j}\frac{E_iE_j}{p^2_{T,jet}})}{dR_L} \quad (1)$$

Theoretically these energy-energy correlators (EECs) are simple objects, represented as light-ray operators in the operator product expansion framework, that allow for the description of all jet substructure observables. Experimentally these energy flow operators are represented by calorimeter cells placed infinitely far away from the interaction point.

A recent analysis of the simplest jet substructure observables, the two-point EEC, was performed using the “MIT open data” from CMS [68]. While no detector corrections were performed, the analysis, demonstrated the power and viability of this type of measurement. Figure 23 shows the R_L weighted two-point EEC correlator (see Eq. 1) as a function R_L. It is helpful to think of this angular separation as a transverse momentum exchange of $\sim p_T^{jet} R_L$ between two hadrons (or tracks or calorimeter towers). The enhanced region at large R_L reflects energy flows between hadrons that were formed from showers that initiated early in the fragmentation process and therefore reflects the perturbative regime of free quarks and gluons. The region of small angular separation is suppressed and corresponds to the regime of confinement or free hadrons. Since the separation R_L^2 is directly proportional to the inverse of the formation time of the hadron, EECs make it possible to image the energy flow of the parton shower as a function of time.

A preliminary analysis of the two point charged hadron EEC at mid-rapidity in $\sqrt{s} = 200$ GeV p+p collisions has been released by the STAR collaboration []. Extending this analysis to $\sqrt{s} = 500$ GeV p+p collisions provides a unique opportunity to study the rapidity dependence as run 22 data utilizes both the upgraded TPC, extending track reconstruction out to $\eta < 1.5$ as well as the recently upgraded forward region $2.5 < \eta < 4$. While it is clear the TPC will be used in the mid-rapidity analysis, more investigations are necessary to understand if the forward analysis should focus only only on the calorimeters (ECAL+HCAL) or also incorporate information from the forward trackers as well. One direction that we would like to explore is the spin dependence of the EECs. Both the 2017 and 2022 datasets include transversely polarized protons at $\sqrt{s} = 510$ GeV and it would be interesting to simply look for any type of spin dependence. The concept of spin dependent EECs is very new and the first paper on the topic, and possible connection to the Collins' functions, has been posted on the archive [69].

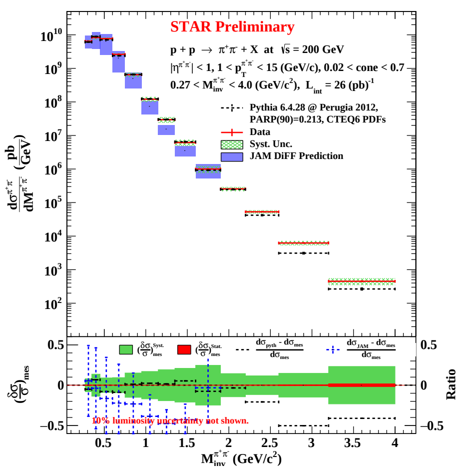

Figure 24: Dihadron cross section extracted from STAR Run 12 $pp\sqrt{s} = 200$ GeV data. Predictions based on Pythia and JAM calculation [70] are compared with the STAR measurement.

Continuing the analysis of the IFF asymmetry, measurements of the unpolarized dihadron cross section are underway at STAR. These measurements will help reduce the theoretical uncertainties, which are dominated by the unpolarized gluon dihadron fragmentation functions in the global analysis. In Fig. 24, the recent JAM prediction based on a collinear calculation at LO [70] is compared to the STAR preliminary result of dipion cross section, obtained from the STAR Run 2012 at 200 GeV. The analysis of IFF asymmetries with more recent STAR data taken in 2017 and 2022 at 510 GeV, together with the data that STAR will record during 2024 at 200 GeV, will provide far more stringent constraints on quark transversities than have been obtained to date when they are included in future global analyses. The enhanced statistical precision, along with implementation of the recent devel-

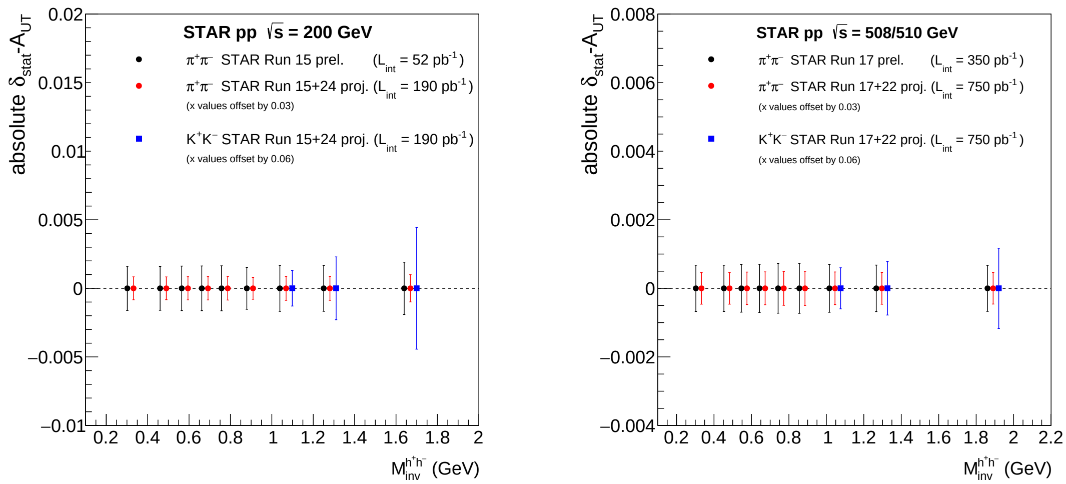

Figure 25: Projected statistical uncertainties for STAR IFF asymmetry measurements for $\pi^+\pi^-$ and K^+K^- pairs at $\eta^{\pi^+\pi^-} > 0$ in p+p at $\sqrt{s} = 200$ (left) and 508/510 GeV (right).

opments in particle identification for hadron-jet measurements, enable exploration of largely unknown strange quark transversity through kaon pair selection. Projections for both dipion and dikaon asymmetries for both 200 and 500 GeV data sets are shown in Fig. 25.

To bring the understanding of the underlying QCD mechanisms of the observed transverse asymmetries at forward rapidities to a new level, the implementation of the Forward Upgrade at STAR in the p+p and p+A running in 2022 and 2024 is absolutely crucial. We will be able to perform measurements with full jets in the forward rapidity region and also the Collins asymmetry with charge separated hadrons, which will provide a much deeper understanding of the underlying QCD mechanism. In addition we will be able to measure A_N for charged hadrons and test theoretical predictions that the underlying mechanism causing the large single spin asymmetries is driven by a novel Collins like fragmentation function couples with transversity.

3.2.3 Opportunities with sPHENIX in $p^{\uparrow}p$ collisions

The strengths of sPHENIX are its capabilities of jet and heavy-flavor reconstruction at mid-rapidity ($|\eta| < 1.1$) with much larger, full 2π coverage acceptance as compared to PHENIX, and at high DAQ rate thanks to the streaming readout, see also Sec. 6.2. This will result in a meaningful advance over previous transversely-polarized 200 GeV $p+p$ data.

The sPHENIX detector saw first $p+p$ collisions with transverse proton polarization in the spring of 2024. In its very first commissioning run in 2023, only part of sPHENIX had been operated successfully. Before the start of the 2024 run, several remedies were incorporated. The 2024 $p+p$ data will be accessible for physics analysis in a time-staggered fashion: the previously already well-commissioned calorimeters will provide clusters almost instantly, while charged-track and jet reconstruction will require also calibrating those tracking detectors that could not be fully commissioned in 2023, and combining the information from all tracking detectors in a coherent way.

With **calorimeter cluster** information only (EMCal clusters with HCals as veto), it will be possible to probe tri-gluon correlators in the collinear twist-3 framework from transverse single-spin asymmetries in neutral-meson and direct-photon production.

Charged-track information will allow the measurement of transverse-single spin asymmetries in inclusive meson production, including open heavy flavor and other neutral mesons with charged decay channels, which will also probe tri-gluon correlators. Single-spin asymmetries in inclusive charged-hadron production in both $p^{\uparrow}p$ and $p^{\uparrow}$Au will allow studying the nuclear dependence of this channel in a unprecedentedly fine binning in p_T and x_F (see also Chap. 4). Di-hadron measurements will probe the transversity PDF and the interference fragmentation function.

With **jet** information, it will be possible to probe the Collins effect via hadron-in-jet measurements. Di-jets, eventually with charge tagging to separate parton flavors, will provide access to the Sivers TMD PDF of valence quarks. Back-to-back jet-photon measurements will probe the Sivers TMD PDF of gluons. Inclusive jet measurements will probe tri-gluon correlators related to the Sivers effect. Charge tagging will also here enable a flavor-separated result

A summary of possible measurements with sPHENIX in $p+p$ collisions with transverse polarization is given in Tab. 1. The time lines for completion of these analyses are discussed in Sec. 5.3.

With these capabilities, the following measurements are planned:

- Transverse single spin asymmetry measurements of neutral pions, direct photons, heavy flavor mesons and charmonia at central rapidities. These measurements select different combinations of the higher twist contributions originating from initial state or final state effects to further decompose their individual contributions. Particularly the direct photon and heavy flavor results are of interest since final state effects are generally

Table 1: Measurement opportunities for transverse single-spin asymmetries A_N at sPHENIX in $p^{\uparrow}p$ collisions at $\sqrt{200}$ GeV including the requirements (x) to reconstructed objects - calorimeter clusters, charged tracks, and jets. "Mesons" also includes heavy flavor and quarkonia.

physics	channel	clusters	tracks	jets
tri-gluon correlator	neutral mesons, direct γ	x		
tri-gluon correlator	mesons	x	x	
transversity PDF, IFF	di-hadrons	x	x	
Collins effect	hadrons-in-jets	x	x	x
Sivers TMD PDF (valence q)	di-jets	x	x	x
Sivers TMD PDF (g)	jet-γ	x	x	x
tri-gluon correlator	inclusive jets	x	x	x

suppressed either by the electromagnetic final state or the dominating hard gluon-gluon interaction, respectively. Because of the latter they will therefore also strongly constrain the so-called tri-gluon correlator that is related to the transverse momentum moment of the gluon Sivers function. The projected uncertainties for direct photon and heavy flavor measurements are shown in Fig. 26.

- Transverse single spin asymmetries of jets at central rapidities. As described above, also jets as a whole are not sensitive to final-state interactions and thus one again is only sensitive to the quark and gluon correlators that are related to their corresponding Sivers function moments.

- Following inclusive jet asymmetry measurements, the next step is the extraction of azimuthal asymmetries of final-state hadrons within the jet as a function of jet transverse momentum, fractional momentum of the hadron relative to the jet momentum, and the transverse momentum of the hadron relative to the jet axis. These follow the description for the STAR measurements above, but the excellent rate capabilities of sPHENIX will allow to improve on the statistical precision at high jet transverse momenta. Given that the underlying transversity distribution is expected to be valence-dominated higher jet momenta relate to higher momentum fractions that are so far only partially accessed by SIDIS measurements. Furthermore, as the hard interactions in hadronic collisions are not governed by the electromagnetic interaction, the intrinsic sensitivity to the down-quark transversity distribution is larger and can help to improve its uncertainties, together with recent COMPASS measurements on a deuteron target [71]. The projected uncertainties are displayed in Fig. 27.

- Quark transversity can also be accessed via di-hadron fragmentation, as described above. The sPHENIX detector will be able to perform the same di-hadron asymmetry measurements for charged hadron pairs, as well as for charged hadron - neutral pion pairs. These measurements provide another collinear way to access the quark transversity functions, making use of the previously measured di-hadron fragmentation measurements from e^+e^- annihilation [72, 73] and global extractions of it [70, 74]. The projected uncertainties for sPHENIX IFF asymmetries for h^+h^- pairs are shown in Fig. 28

- Nearly back-to-back di-jet, photon-jet and heavy-flavor pair asymmetry measurements provide another clean access to intrinsic transverse momentum dependent functions since the transverse momentum of the pair is accessible in addition to the hard scale given by the jet transverse momentum or di-jet mass. Therefore TMD factorization is in principle applicable but not necessarily valid in this process. As described above, performing these measurements in transversely polarized collisions thus gives access to the Sivers functions. Using the different types of final states, as well as enhancing certain parton flavors via jet-charge and other sub-structure selections provides additional sensitivity to different quark flavors and gluons.

In addition to these proton-spin-dependent signatures, a number of measurements that do not require beam polarization are possible at sPHENIX with $p+p$ and $p+$A collisions, for example, hadronization studies. More details are given in Sec. 4.2.3.

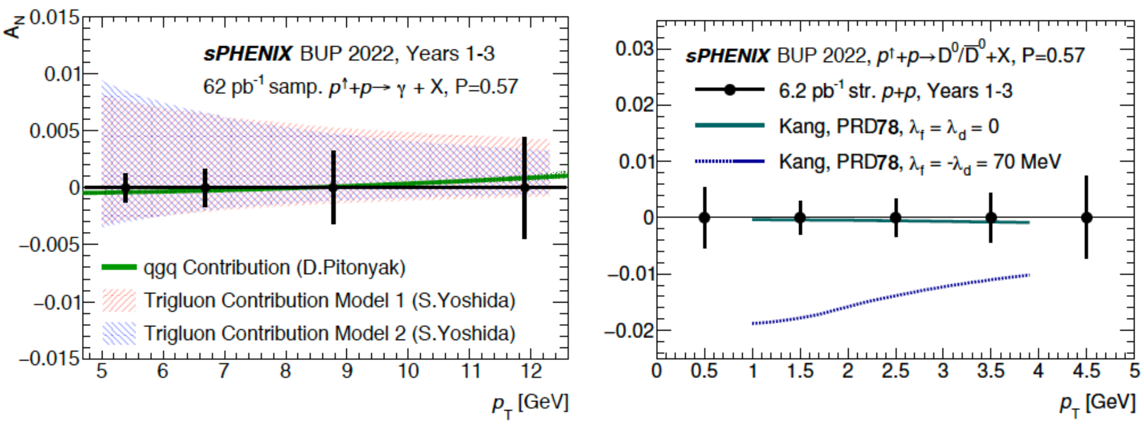

Figure 26: Projected statistical uncertainties for direct photon (left) and D^0 mesons (right) A_N with sPHENIX, compared with twist-3 model calculations based on [62, 75] and [64], respectively.

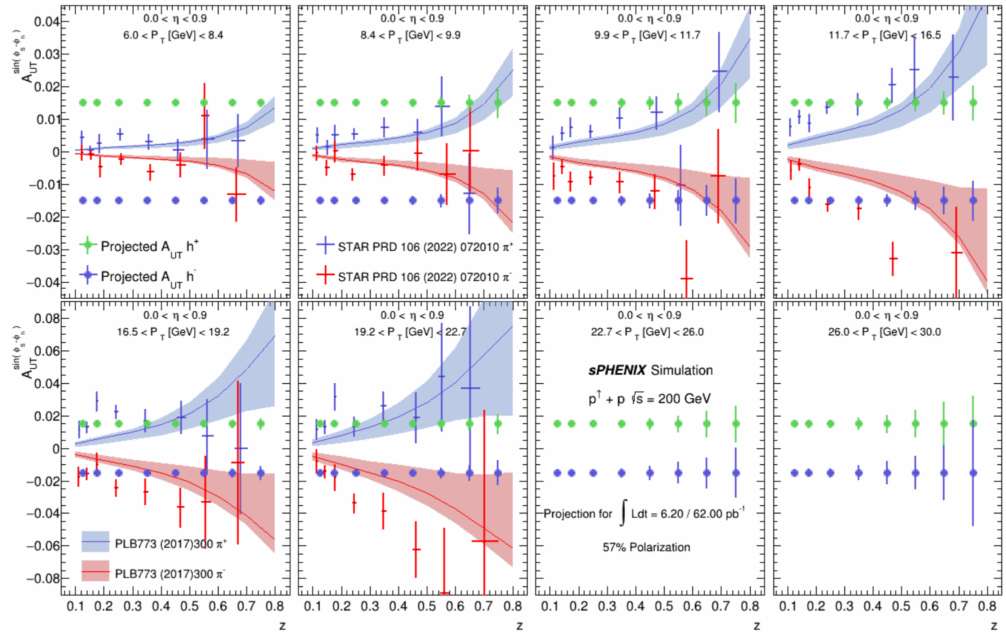

Figure 27: Projected statistical uncertainties for sPHENIX hadron-in-jet Collins asymmetries for h^+ and h^-, as a function of hadron fractional momentum z in bins of jet transverse momentum. The data was projected to be collected with calorimetry-based jet triggers for jet transverse momenta above 10 GeV and with streaming readout below. The data is compared to existing STAR measurements [36](red and violet data points) and calculations from [37] (red and violet error bands).

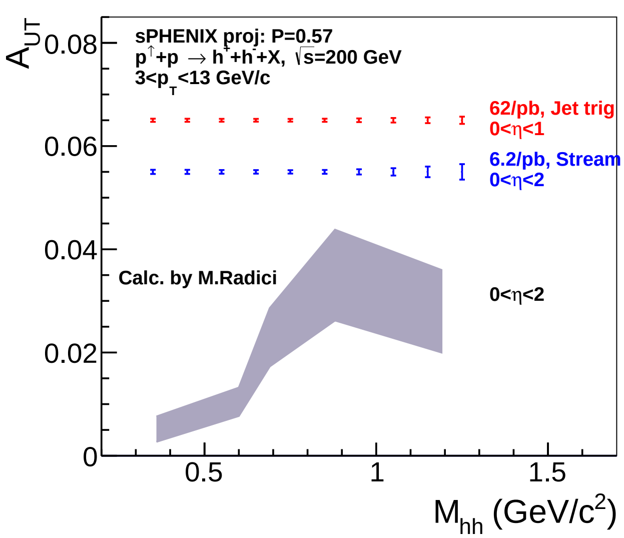

Figure 28: Projected statistical uncertainties for sPHENIX IFF asymmetry measurements for h^+h^- pairs, collected with calorimetry-based jet trigger and with streaming readout. The grey uncertainty band represents the asymmetry prediction based on the global analysis of ref [49], provided by M.Radici.

4 Cold QCD Physics with Nuclear Beams

Our quest to understand QCD processes in Cold Nuclear Matter (CNM) centers on the following fundamental questions:

- Can we experimentally find evidence of a novel universal regime of non-linear QCD dynamics in nuclei?
- What is the role of saturated strong gluon fields, and what are the degrees of freedom in this high gluon density regime?
- What is the fundamental quark-gluon structure of light and heavy nuclei?
- Can a nucleus, serving as a color filter, provide novel insight into the propagation, attenuation and hadronization of colored quarks and gluons?

Various aspects of these questions have been addressed by numerous experiments and facilities around the world, most of them at significantly lower center-of-mass energies and kinematic reach than RHIC. Deep inelastic scattering on nuclei addresses some of these questions with results from, for instance, HERMES at DESY [76–78], CLAS at JLab [79], and in the future from the JLab 12 GeV. This program is complemented by hadron-nucleus reactions in fixed target p+A at Fermilab (E772, E886, and E906) [80] and at the CERN-SPS.

In the following we propose a measurement program unique to RHIC to constrain the initial state effects in strong interactions in the nuclear environment. We also highlight the complementarity to the LHC p+Pb program and stress why RHIC data are essential and unique in the quest to further our understanding of nuclei. The uniqueness of the RHIC program is based on the flexibility of the RHIC accelerator to run collisions of different particle species at very different center-of-mass energies. This in combination with the enhanced STAR detector capabilities in Run-24/25 allows to disentangle nuclear effects in the initial and final state as well as leading twist shadowing from saturation effects in a kinematic regime where all these effects are predicted to be large. Most of the discussed measurements critically rely on the Forward Upgrade.

4.1 Achievements To-Date

4.1.1 Nuclear parton distribution functions

A main emphasis of the Run-15 and later p+A runs is to determine the initial conditions of the heavy ion nucleus before the collision to support the theoretical understanding of the A+A program both at RHIC and the LHC. In the following, the current status of nPDFs will be discussed, including where the unique contributions of RHIC lie, in comparison to the LHC and the future EIC.

Our current understanding of nuclear parton distribution functions (nPDFs) is still very limited, in particular, when compared with the rather precise knowledge of PDFs for free protons collected over the past 30 years. Figure 29 shows an extraction of nPDFs from

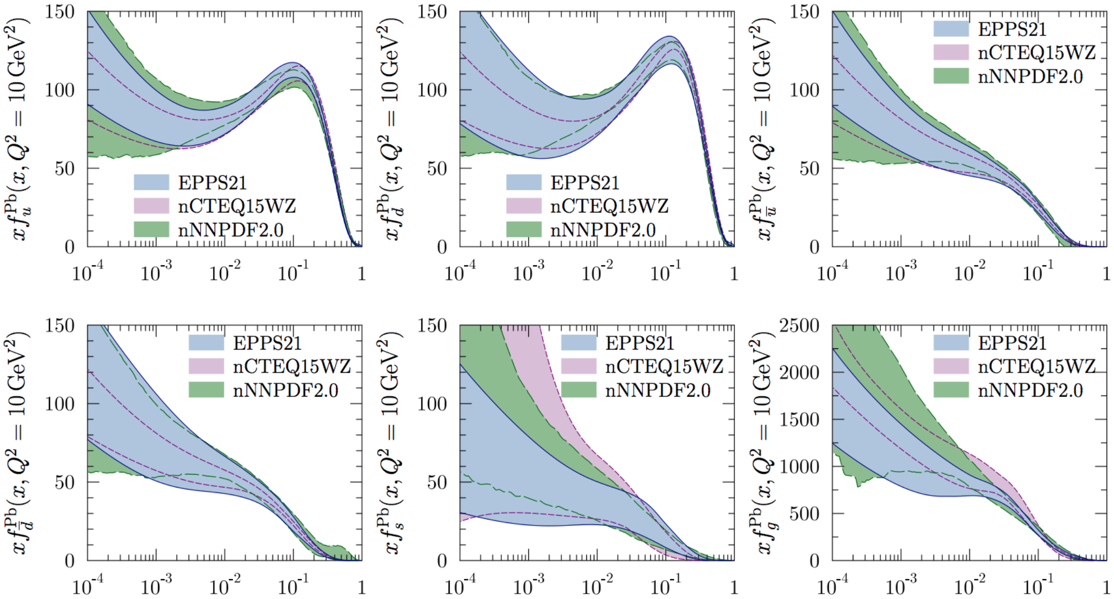

Figure 29: Summary of the most recent sets of nPDFs at 90% confidence-level. [81]

available data, along with estimates of uncertainties. All results are shown in terms of the nuclear modification ratios, i.e., scaled by the respective PDF of the free proton. The kinematic coverage of the data used in the EPPS21 fits [81] are shown in Fig. 30. Clearly, high precision data at small x and for various different values of Q^2 are needed to better constrain the magnitude of suppression in the x region where non-linear effects in the scale evolution are expected. In addition, such data are needed for several different nuclei, as the A-dependence of nPDFs cannot be predicted from first principles in pQCD and, again, currently relies on assumptions. The PHENIX midrapidity $\pi^0 R_{dAu}$ data [82], are the only data which can probe the gluon in the nucleus directly, but these data also suffer from unknown nuclear effects in the final state (see [83]). Therefore, it is critical to have high precision data only sensitive to nuclear modification in the initial state over a wide range in x and intermediate values of Q^2 (away from the saturation regime) to establish the nuclear modification of gluons in this kinematic range.

It is important to realize that the measurements from RHIC are compelling and essential even when compared to what can be achieved in p+Pb collisions at the LHC. Due to the higher center-of-mass system energy most of the LHC data have very high Q^2, where the nuclear effects are already reduced significantly by evolution and are therefore very difficult to constrain.

RHIC has the *unique* capability to provide data in a kinematic regime (moderate Q^2 and medium-to-low x) where the nuclear modification of the sea quark and the gluon is expected to be sizable. In addition, and unlike the LHC, RHIC has the potential to vary the nucleus in p+A collisions and as such also constrain the A-dependence of nPDFs.

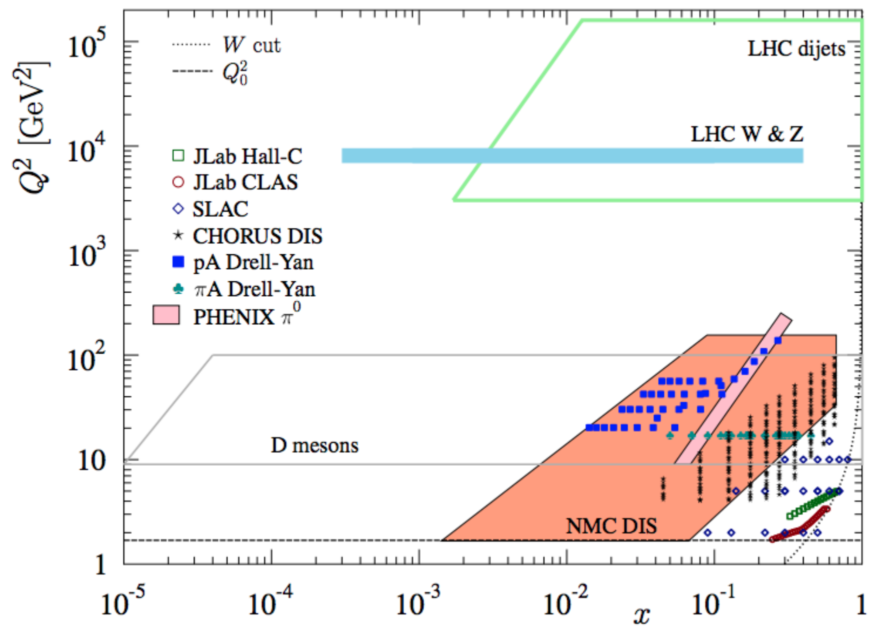

Figure 30: The kinematic x and Q^2 coverage of data used in the EPPS21 nPDF fits. [81]

Extraction of this information is less ambiguous if one uses processes in which strong (QCD) final-state interactions can be neglected or reduced. Such golden channels would include a measurement of R_{pA} for Drell-Yan production at forward pseudo-rapidities with respect to the proton direction ($2.5 < \eta < 4$) to constrain the nuclear modifications of sea-quarks. Moreover, the R_{pA} for direct photon production in the same kinematic regime will help constrain the nuclear gluon distribution. Data for the first measurement of R_{pA} for direct photon production have already been taken during the p+Au and p+Al Run-15, with recorded luminosities by STAR of $L_{pAu} = 0.45$ pb^{-1} and $L_{pAl} = 1$ pb^{-1}, respectively. Like all other inclusive probes in p+p and p+A collisions, e.g., jets, no access to the exact parton kinematics can be provided event-by-event but global QCD analyses easily account for that. After the p+Au Run-24/25, the statistical precision of the prompt photon data will be sufficient to contribute to a stringent test of the universality of nuclear PDFs when combined with the expected data from the EIC (see Figure 2.22 and 2.23 in Ref [84]). The Forward Upgrade with its tracking at forward rapidities will also provide the possibility to measure R_{pA} for positive and negatively charged hadrons. Approximately equal nucleon-nucleon luminosities for p+p and p+Au are important for the optimization of R_{pA} measurements as they directly compare the same observable yields in both collision systems.

Figure 31 shows the kinematic coverage in $x - Q^2$ of past, present, and future experiments capable of constraining nuclear parton distribution functions. The shown experiments provide measurements that access the initial state parton kinematics on an event-by event basis (in a leading order approximation) while remaining insensitive to any nuclear effects in the final state. Some of the LHC experiments cover the same x-range as DY at forward

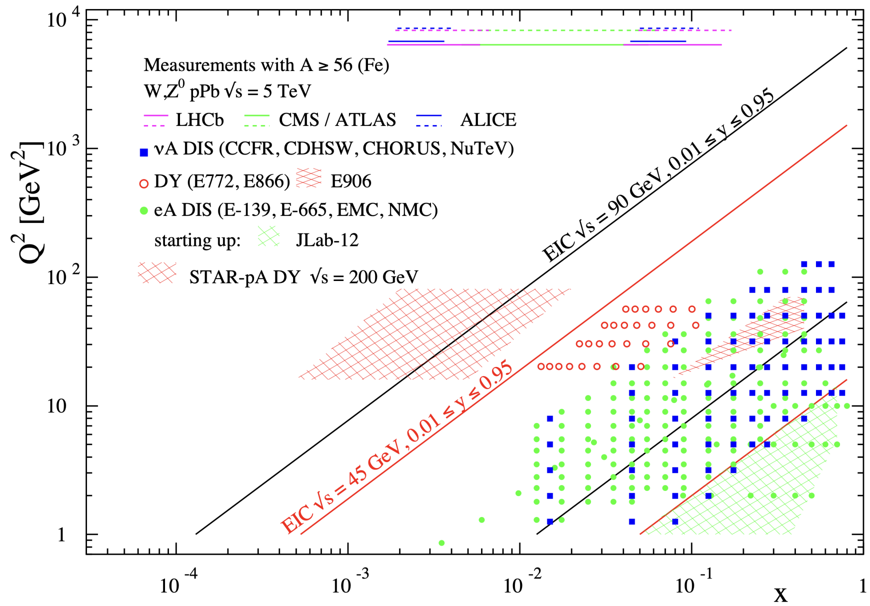

Figure 31: The kinematic coverage in $x - Q^2$ of past, present and future experiments constraining nPDFs with access to the exact parton kinematics event-by-event and no fragmentation in the final state.

pseudo-rapidities at RHIC but at a much higher scale Q^2, where nuclear modifications are already significantly reduced [85–87]. At intermediate Q^2, DY at STAR will extend the low-x reach by nearly one decade compared to EIC.

The biggest challenge of a DY measurement is to suppress the overwhelming hadronic background: the total DY cross-section is about 10^{-5} to 10^{-6} smaller than the corresponding hadron production cross-sections. Therefore, the probability of misidentifying a hadron track as a lepton has to be suppressed to the order of 0.1% while maintaining reasonable electron detection efficiencies. To that end, we have studied the combined electron/hadron discriminating power of the Forward Upgrade. It was found that by applying multivariate analysis techniques to the features of EM/hadronic shower development and momentum measurements we can achieve hadron rejection powers of 200 to 2000 for hadrons of 15 GeV to 50 GeV with 80% electron detection efficiency.

The potential impact of the DY R_{pA} data for the EPPS-19 sets of nPDFs was studied through a re-weighting procedure [88]. We expect a significant impact on the uncertainties of R_{pA} DY upon including the projected and properly randomized data. Clearly, the DY data from RHIC will be instrumental in reducing present uncertainties in nuclear modifications of sea quarks. Again, these data will prove to be essential in testing the fundamental universality property of nPDFs in the future when EIC data become available.

STAR's unique detector capabilities provide data on J/Ψ-production in ultra-peripheral collisions. This measurement can provide access to the spatial gluon distribution by measuring the t-dependence of $d\sigma/dt$. To study the gluon distribution in the gold nucleus, events need to be tagged where the photon is emitted from the proton (γ+Au→ J/ψ). However, with the signal-to-background ratio in p+Au collisions (see the contribution from the γ+Au→ J/ψ process and the background processes in Fig. 35), we expect much better sensitivity to the gluon distributions in Au from the Au+Au program. In addition to

J/ψ photoproduction in UPC for exclusive reactions, photoproduction of back-to-back jets is also sensitive the PDFs (nPDFs in Au+Au UPC). This measurement has never been performed at RHIC experiments, where the kinematic coverage can go to moderate to high-x. The anti-shadowing region in nuclei, for example, is of great interest by comparing to this measurement in the proton. Furthermore, we can possibly extend the measurement from inclusive photoproduction dijets to diffractive dijets in $p+p$ and $p+$Au collisions, which will be sensitive to the QCD factorisation breaking [89]. For details, see Sec. 4.1.3 for discussion in UPCs.

4.1.2 Non-linear QCD effects

Our understanding of the proton structure and of the nuclear interactions at high energy would be advanced significantly with the definitive discovery of the saturation regime [90–96]. Saturation physics would provide an infrared cutoff for perturbative calculations, the saturation scale Q_s, which grows with the atomic number of the nucleus A and with decreasing value of x. If Q_s is large it makes the strong coupling constant small, $\alpha_s(Q_s^2) << 1$ allowing for perturbative QCD calculations to be under theoretical control.

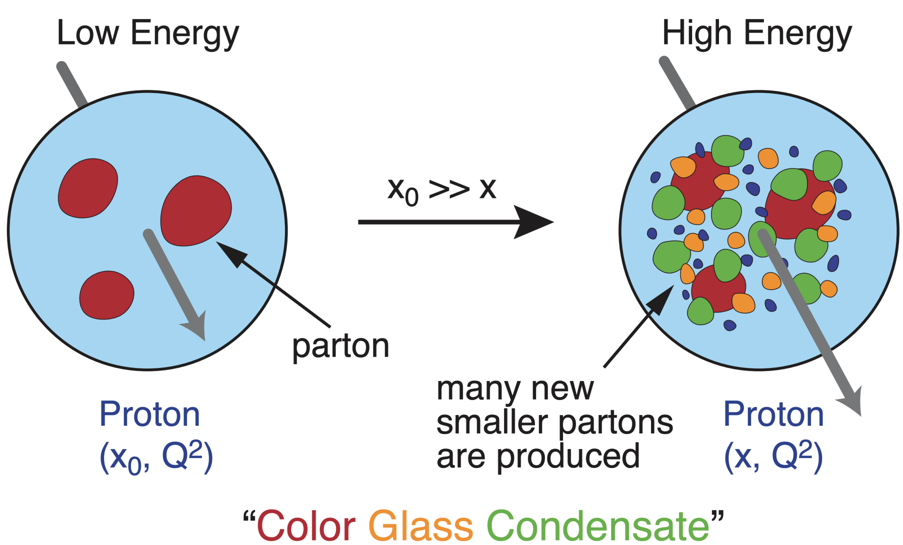

Figure 32: Proton wave function evolution towards small-x.

It is well known that PDFs grow at small-x. If one imagines how such a high number of small-x partons would fit in the (almost) unchanged proton radius, one arrives at the picture presented in Fig. 32: the gluons and quarks are packed very tightly in the transverse plane. The typical distance between the partons decreases as the number of partons increases, and can get small at low-x (or for a large nucleus instead of the proton). One can define the saturation scale as the inverse of this typical transverse inter-parton distance. Hence Q_s indeed grows with A and decreasing x.

The actual calculations in saturation physics start with the classical gluon fields (as gluons dominate quarks at small-x) [97–103], which are then evolved using the nonlinear

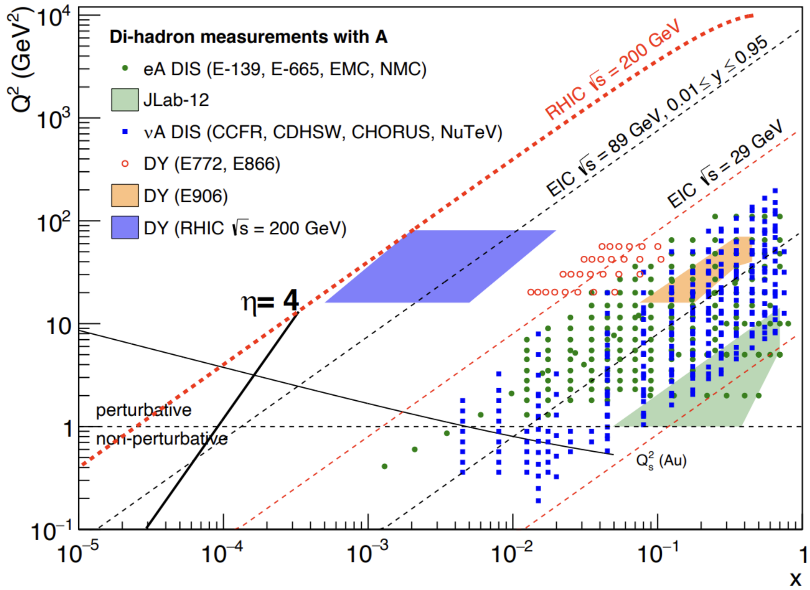

Figure 33: Kinematic coverage in the $x-Q^2$ plane for p+A collisions at RHIC, along with previous e+A measurements, the kinematic reach of an electron-ion collider, and estimates for the saturation scale Q_s in Au nuclus and the line illustrating the range in x and Q^2 covered with hadrons at rapidity $\eta = 4$.

small-x BK/JIMWLK evolution equations [104–113]. The saturation region can be well-approximated by the following formula: $Q_s^2 \sim (A/x)^{1/3}$. Note again that at small enough x the saturation scale provides an IR cutoff, justifying the use of perturbative calculations. This is important beyond saturation physics, and may help us better understand small-x evolution of the TMDs.

While the evidence in favor of non-linear QCD effects has been gleaned from the data collected at HERA, RHIC and the LHC, the case for saturation is not sealed and alternative explanations of these data exist. The EIC is slated to provide more definitive evidence for saturation physics [114]. To help the EIC complete the case for saturation, it is mandatory to generate higher-precision measurements in p+Au collisions at RHIC. These higher-precision measurements would significantly enhance the discovery potential of the EIC as they would enable a stringent test of universality of the CGC. We stress again that a lot of theoretical predictions and results in the earlier Sections of this document would greatly benefit from this physics: the small-x evolution of TMDs in a longitudinally or transversely polarized proton, or in an unpolarized proton, can all be derived in the saturation framework [115] in a theoretically better-controlled way due to the presence of Q_s. Hence non-linear QCD effects may help us understand both the quark and gluon helicity PDFs as well as the Sivers and Boer-Mulders functions.

The saturation momentum is predicted to grow approximately like a power of energy, $Q_s^2 \sim E^{\lambda/2}$ with $\lambda \sim 0.2-0.3$, as phase space for small-x (quantum) evolution opens up. The saturation scale is also expected to grow in proportion to the valence charge density at the onset of small-x quantum evolution. Hence, the saturation scale of a large nucleus should exceed that of a nucleon by a factor of $A^{1/3} \sim 5$ (on average over impact parameters). RHIC is capable of running p+A collisions for different nuclei to check this dependence on the mass number. This avoids potential issues with dividing, e.g., p+Pb collisions in

N_{part} classes [116]. Figure 33 shows the kinematic coverage in the $x - Q^2$ plane for p+A collisions at RHIC, along with previous e+A measurements and the kinematic reach of an EIC. The saturation scale for a Au nucleus is also shown. To access at RHIC a kinematic regime sensitive to non-linear QCD effects with $Q^2 > 1$ GeV^2 requires measurements at forward rapidities. For these kinematics the saturation scale is moderate, on the order of a few GeV^2, so measurements sensitive to non-linear QCD effects are by necessity limited to semi-hard processes.

Until today the golden channel at RHIC to observe strong hints of non-linear QCD effects has been the angular dependence of two-particle correlations, because it is an essential tool for testing the underlying QCD dynamics [116]. In forward-forward correlations facing the $p(d)$ beam direction one selects a large-x parton in the $p(d)$ interacting with a low-x parton in the nucleus. For $x < 0.01$ the low-x parton will be back-scattered in the direction of the large-x parton. Due to the abundance of gluons at small x, the backwards-scattered partons are dominantly gluons, while the large-x partons from the $p(d)$ are dominantly quarks. The measurements of di-hadron correlations by STAR and PHENIX [117, 118], have been compared with theoretical expectations using the CGC framework based on a fixed saturation scale Q_s and considering valence quarks in the deuteron scattering off low-x gluons in the nucleus with impact parameter $b = 0$ [119,120]. Alternative calculations [121] based on both initial and final state multiple scattering that determine the strength of this transverse momentum imbalance, in which the suppression of the cross-section in d+Au collisions arises from cold nuclear matter energy loss and coherent power corrections, have also been very successful to describe the data.

The p+A Run-15 at RHIC has provided unique opportunities to study this channel in more detail at STAR. The high delivered integrated luminosities allow one to vary the trigger and associated particle p_T from low to high values and thus crossing the saturation boundary as shown in Fig. 33 and reinstate the correlations for central p+A collisions for forward-forward π^0's. Studying di-hadron correlations in p+A collisions instead of d+A collisions has a further advantage. In reference [122], the authors point out that the contributions from double-parton interactions to the cross-sections for $dA \rightarrow \pi^0\pi^0 X$ are not negligible. They find that such contributions become important at large forward rapidities, and especially in the case of d+A scattering. The recent published forward di-π^0 correlation measured by the STAR detector pioneered the observation of the dependence of nonlinear gluon dynamics on the nuclear mass number A [123], see the left panel of Fig. 34. The area is extracted by a Gaussian fit of the back-to-back correlation measured from each collision system. The area ratio of p+A/p+p presents the relative yields of back-to-back di-π^0s in p+A with respect to p+p collisions. The area ratio in p+Au over p+p is about 50% indicating a clear suppression of back-to-back di-π^0 correlation in p+Au compared to p+p collisions. The same trend but smaller amount of suppression is observed in p+Al collisions. This behavior is consistent with different calculations based on the CGC formalism and is a clear hint of non-linear effects. The suppression is found to scale with A and linearly dependent on $A^{1/3}$. The extracted slope from the linear dependence will be a critical input for the gluon saturation model in CGC.

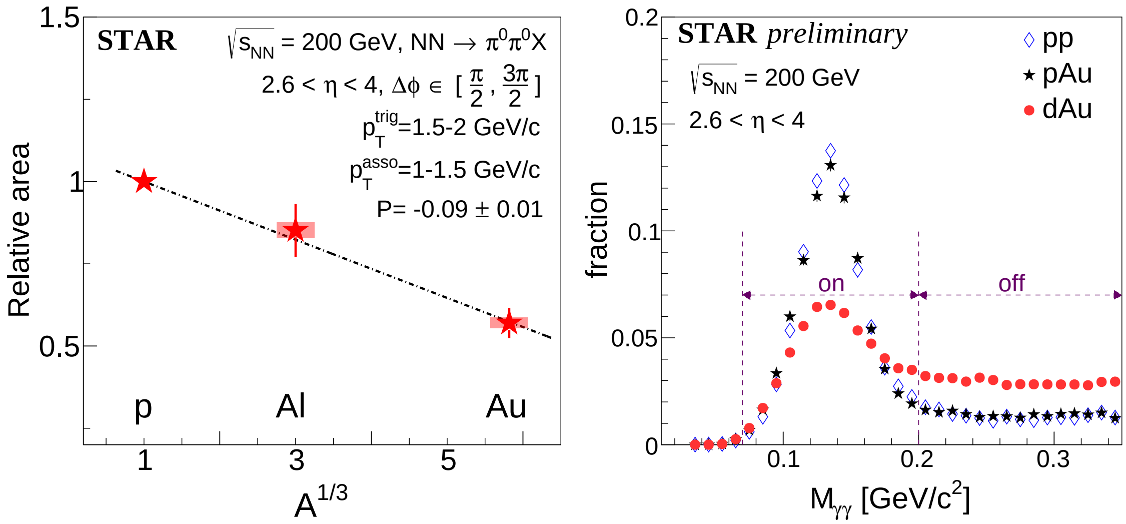

Figure 34: Left: Relative area of back-to-back di-π^0 correlations at forward pseudorapidities ($2.6 < \eta < 4.0$) in p+Au and p+Al relative to p+p collisions for $p_T^{\rm trig} = 1.5{-}2$ GeV/c and $p_T^{\rm asso} = 1{-}1.5$ GeV/c. The vertical bars for the Al and Au ratios indicate the statistical uncertainties and the vertical bands indicate the systematic uncertainties. The data points are fitted by a linear function, whose slope (P) is found to be -0.09 ± 0.01. Right: The invariant mass spectra for di-photon in p+p, p+Au, and d+Au. The on mass range is chosen as 0.07-0.2 GeV/c^2, the off mass range is 0.2-0.35 GeV/c^2.

A comparison between p+p (Run-15), p+Au (Run-15), and d+Au (Run-16) collisions can help provide insight into the contributions from multiple parton scattering [122]. Figure 34 right shows the invariant mass spectra for final p+p and p+Au results and the preliminary d+Au. It is clear from the comparison that there is significantly more background in the the d+Au data than the p+p and p+Au data. This combinatoric correlation dominates in d+Au collisions, which makes it very challenging to identify the signal correlation. The forward di-π^0 correlation measurement favors the cleaner p+Au collisions rather than d+A collisions. It emphasizes the importance of measuring the di-hadron correlation in p+A collisions with the STAR Forward Upgrade in the future Run-24/25. Run-24/25 will be able to study more luminosity-hungry processes and/or complementary probes to the di-π^0 correlations, i.e. di-hadron correlations for charged hadrons, photon-jet, photon-hadron and di-jet correlations. Utilizing the forward tracking systems, the background for particle identification will be much suppressed with respect to the current di-π^0 studies. The detailed projection plots will be presented in Sec. 4.2.2.

4.1.3 Ultra-peripheral collisions

Constraints on GPDs have mainly been provided by exclusive reactions in deep inelastic scattering (DIS), e.g. deeply virtual Compton scattering. RHIC, with its unique capability to collide transversely polarized protons at high energies, has the opportunity to measure A_N for exclusive J/ψ production in ultra-peripheral collisions (UPCs) [124]. In such a UPC process, a photon emitted by the opposing beam particle (p or A) collides with the polarized proton. The measurement is at a fixed $Q^2 \sim M^2_{J/\psi} \approx 10$ GeV^2 and $10^{-4} < x < 10^{-1}$. A nonzero asymmetry would be the first signature of a nonzero GPD E_g for gluons, which is sensitive to spin-orbit correlations and is intimately connected with the orbital angular momentum carried by partons in the nucleon and thus with the proton spin puzzle.

The Run-15 $p^{\uparrow}Au$ data allowed a proof-of-principle of such a measurement. A trigger requiring back-to-back energy deposits in the Barrel Electromagnetic Calorimeter selected J/ψ candidates. The e^+e^- mass distribution after selection cuts is shown in the left of Fig. 35, and the pair p_T distribution of the J/ψ mass peak is shown on the right of that figure. The data are well described by the STARlight model [125] (colored histograms in the figure), including the dominant $\gamma{+}p^{\uparrow} \rightarrow J/\psi$ signal process and the $\gamma{+}Au \rightarrow J/\psi$ and $\gamma{+}\gamma{\rightarrow}e^+e^-$ background processes. The left of Fig. 36 shows the STAR preliminary measurement (solid circle marker) of the transverse asymmetry A_N^{γ} for the J/ψ signal, which has a mean photon-proton center-of-mass energy $W_{\gamma p} \approx 24$ GeV. The result is consistent with zero. Also shown is a prediction based on a parameterization of E_g [126]; the present data provide no discrimination of this prediction.

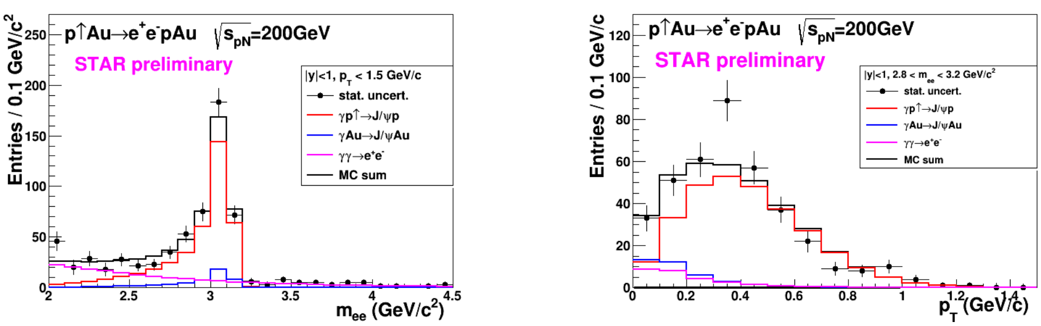

Figure 35: Mass distribution of selected e^+e^- pairs (left), and p_T distribution of the J/ψ mass peak (right). The colored histograms are the indicated processes modelled by STARlight and the sum fit to the data.

This measurement can be greatly improved with a high statistics transversely polarized $p^{\uparrow}Au$ Run-24. The integrated luminosity for the Run-15 measurement was 140 nb^{-1}; Run-24 will provide about 1.2 pb^{-1}, allowing a sizeable reduction of statistical uncertainty in the same $W_{\gamma p}$ range. In addition, the Forward Upgrade and iTPC will provide a significant extension of the $W_{\gamma p}$ range of the measurement. The right panel of Fig. 36 shows the accepted cross section for $\gamma{+}p^{\uparrow} \rightarrow J/\psi$ for various detector pseudorapidity ranges. With the full detector, the sensitive cross section is a factor of five times the central barrel alone. Also, the accepted region has a lower mean $W_{\gamma p} \approx 14$ GeV. Predictions based on E_g parameterizations such as shown in the figure have a larger asymmetry at lower $W_{\gamma p}$, with increased possibility of a nonzero result. The projected statistical uncertainty on A_N^{γ} is shown in the left of

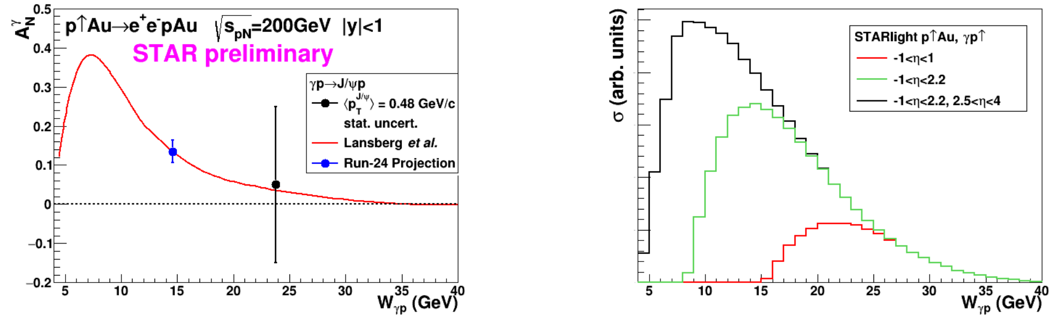

Figure 36: Left: The measured J/ψ transverse asymmetry A_N^γ and a prediction based on a parameterization of E_g. Right: The accepted cross section for $\gamma + p^\uparrow \to J/\psi$ for various detector pseudorapidity η ranges; the black curve shows the result for the full STAR detector with the Forward Upgrade and the iTPC.

Fig. 36 (blue square marker), offering a powerful test of a non-vanishing E_g. Alternatively, the increased statistics will allow a measurement of A_N^γ in bins of $W_{\gamma p}$.

The UPC cross section scales with $\sim Z^2$ of the the nucleus emitting the photon; for protons this is $1/79^2$ relative to Au nuclei, which makes analogous measurements in p+p collisions extremely luminosity-hungry. Therefore, the p+Au run is important for this measurement.

4.1.4 Nuclear dependence of single spin asymmetries

In 2015, RHIC also investigated polarized proton-nucleus collisions with either Al or Au beams. These have been utilized to study the A dependence of the nonzero single-spin asymmetries that were observed for hadrons in the forward region. In PHENIX the asymmetries for charged hadrons at rapidities of 1.2 to 2.4 were studied. A strong nuclear dependence was observed that was consistent with an $A^{-1/3}$ suppression for positive hadrons [127], as shown in Fig. 37. A similar suppression is also seen as a function of the centrality of the collisions.

STAR has also published the A dependence for neutral pions at forward rapidities of 2.7 to 3.8 and higher x_F that also show a suppression of the asymmetries [51]. However, in that rapidity region the suppression appears much smaller than seen by PHENIX, as seen in Fig. 38. The initial motivation for studying the nuclear dependence of the single-spin asymmetries originates from possible saturation effects on these asymmetries, but it has since been realized that the presented measurements neither reach x nor scales that are low enough for such effects to be relevant [128]. As such, there is at present no clear understanding of the mechanism that produces the suppression of these asymmetries.

The data to be collected by sPHENIX in p+p and p+Au collisions would not only considerably improve the precision of PHENIX measurements for charged hadron TSSA (Fig. 37),

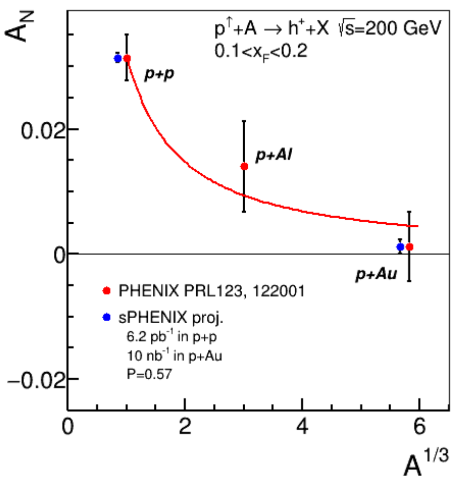

Figure 37: A dependence of transverse single-spin asymmetries of positively charged hadrons at $\sqrt{s} = 200$ GeV at pseudo-rapidities of 1.2 to 2.4 measured at PHENIX [127], and sPHENIX projected uncertainties for data to be collected with streaming readout.

but also allow for fine binning of TSSA in p_T and x_F in extended ranges. That will provide invaluable information for studying rich phenomena behind TSSA in hadronic collisions, utilizing RHIC's unique capabilities to collide high energy polarized protons and heavy nuclei.

In the far forward region also the nuclear dependence of neutron asymmetries was extracted as a function of transverse momentum and the longitudinal momentum fraction [129, 130]. Neutron asymmetries in proton-proton collisions can be described by the interference of pion and other meson interactions between the two colliding nucleons [131] and are found to be negative. In contrast, the p+Al asymmetries are on average close to zero, while the p+Au asymmetries change sign and have a significantly larger magnitude. It was found that the origin of this nuclear dependence originates from the additional contribution of ultra-peripheral collisions that increase quadratically with the charge of the nucleus [132]. When correlating the asymmetries with event activity related to hadronic activity, one indeed sees that the asymmetries remain negative while the events more likely to originate from ultra-peripheral collisions show even larger, positive asymmetries already for p+Al collisions.

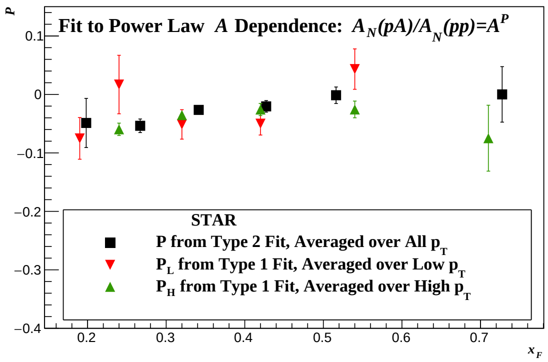

Figure 38: The exponent, P, for nuclear A dependence of the π^0 transverse single-spin asymmetry ratio of p+A to p+p as a function of x_F at $\sqrt{s}$ = 200 GeV at $2.7 < \eta < 3.8$ at STAR [51]. The main difference of two types of fits is with and without correlated uncertainties.

4.2 Future Results

According to the recommendations of the Nuclear and Particle Physics Program Advisory Committee (PAC) for RHIC, the top priority for Run-24 is completing the commissioning of sPHENIX and collecting the high statistics p+p dataset that is the necessary reference for all the sPHENIX hard probes Au+Au measurements to come in Run-25 and that will at the same time allow STAR to make landmark polarized proton measurements using its new forward instrumentation. The second priority for Run-24 is p+Au running in Run-24 if, and only if, the top priority above has been completed and a p+Au run of 5 weeks can be accomplished. If the p+Au run is not done in Run-24 there will be a compelling case for running RHIC beyond the completion of the Run-25 Au+Au data-taking in order to include at least five weeks of p+Au running, even if doing so extends Run-25 beyond June 2025. These p+p and possible p+Au datasets will provide the opportunities to further explore the nuclear modifications at both initial- and final-state at RHIC.

4.2.1 PHENIX

The forward calorimeter extension with preshower detector MPC-EX enabled the identification and reconstruction of prompt photons and π^0s at energies up to 80 GeV. The MPC-EX was available in Run-16 d+Au data, which is expected to contribute critical results that will help to further elucidate the gluon distribution at low-x in nuclei. The ongoing analysis includes the development of unique techniques for MPC-EX data analysis and extensive simulation of detector performance.

4.2.2 STAR

The high luminosity p+p data collected in 2024 and possible p+Au data to be collected in 2024 or 2025 will be ideal to continue the correlation measurements in searching for gluon saturation. To compare with the published results on di-π^0 correlations from 2015 data, the statistical projections of di-π^0 and di-$h^{\pm}$ measurements for Run-24 p+p and Run-24/25 p+Au data are shown in Fig. 39 with various assumptions.

Table 2: Five scenarios for the data taking during Run-24 p+p and possible p+Au data from Run-24/25. Note that a set-up time of 5.5 weeks was assumed. We considered three conditions for the total Cyro weeks as 28, 24, and 20.

Scenarios	Cryo weeks [w]	Set-up [w]	p+p [w]	p+A [w]	Details
S0	28	5.5	12	10.5	equal nucleon-nucleon luminosity
S1	28	5.5	11.3	11.2	equal time
S2	28	5.5	17.5	5	request from the last PAC
S3	24	5.5	9.5	9	equal nucleon-nucleon luminosity
S4	20	5.5	7.5	7	equal nucleon-nucleon luminosity

In Fig. 39, the back-to-back di-π^0 and di-$h^{\pm}$ yields in p+Au with respect to p+p collisions are presented as a function of the associated particle's p_T. The black open circles represent the data points published with Run-15 data with only statistical errors [123]. The rest are the projected statistical errors for Run-24/25, with the central value located on the fitting function from the Run-15 data.

Figure 39(right) presents the projected statistical errors for the di-$h^{\pm}$ channel, which is the golden channel to quantitatively probe gluon saturation. The forward tracking system enables us to detect charged hadrons in the forward region ($2.6 < \eta < 4.0$) at low p_T (down to 0.2 GeV/c). Lower p_T enables us to probe the lower x region in the phase space, where saturation is predicted to be stronger. So, with this channel, we are expecting to observe the largest suppression of the back-to-back di-$h^{\pm}$ correlations in p+Au with respect to p+p collisions at RHIC energy. With enough statistics for Run-24/25, STAR can further investigate the nonlinear QCD phenomena in the region closer to gluon saturation, where Run-15 data cannot access. In Fig.39(right), the statistical errors are estimated through a different way compared to the di-π^0 channel, as for low p_T (< 1 GeV/c) we will use min-bias triggered data and for high p_T (> 1 GeV/c) we will use high-p_T data triggered by the forward calorimeters. Considering the prescale, we used the estimated number of events for Run-24/25 compared with the number of events recorded in Run-15 for both p+p and p+Au collisions, to calculate the statistical errors of Run-24/25. The number of events for Run-24/25 is

$$N_{evt} = \text{event rate} \times N_{week} \times N_{day} \times N_{min} \times N_{sec} \times t_{up} \times t_{live} \times eff_{trk} \quad (2)$$

where the recorded min-bias event rate is assumed to be 500 Hz, $t_{up} = 50\%$, $t_{live} = 70\%$, and the tracking efficiency is $eff_{trk} = 90\%$. Since the yield of di-$h^{\pm}$ pairs is much larger than di-π^0, overall we will obtain much smaller statistical errors for the Run-24/25 di-$h^{\pm}$ channel compared to di-π^0 results from Run-15.

It is important to note that for the measurements to date in $p(d)$+A collisions both initial and final states interact strongly, leading to severe complications in the theoretical treatment (see [134, 135], and references therein). As described in detail in the Section above, in p+Au

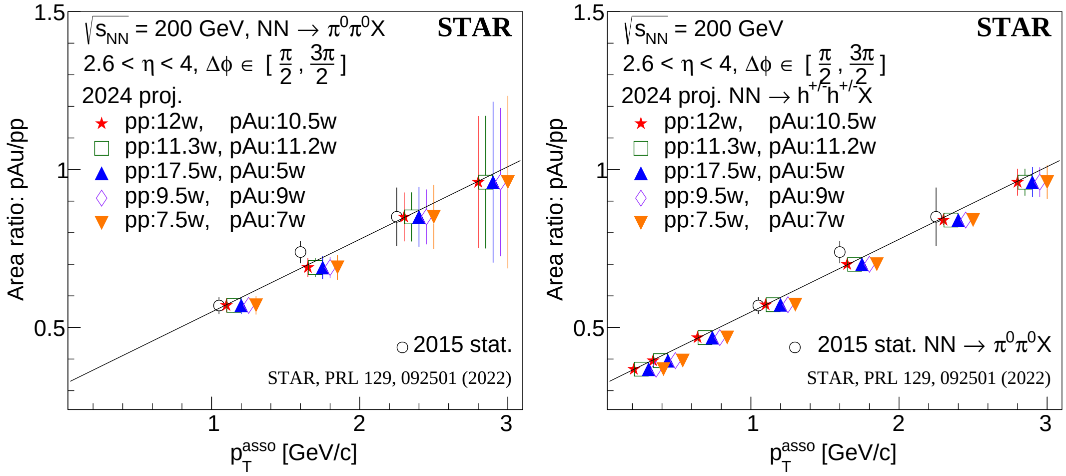

Figure 39: Relative area of back-to-back di-π^0 (Left) and di-$h^{\pm}$ (Right) correlations at forward pseudorapidities ($2.6 < \eta < 4.0$) in Run-24/25 p+Au with respect to Run-24 p+p collisions, in comparison with the published Run-15 di-π^0 results. The black open circles represent the published Run-15 di-π^0 data points with statistical errors only. The rest of the data points come from the projected statistical errors under different data-taking assumptions (Tab. 2) for Run-24/25.

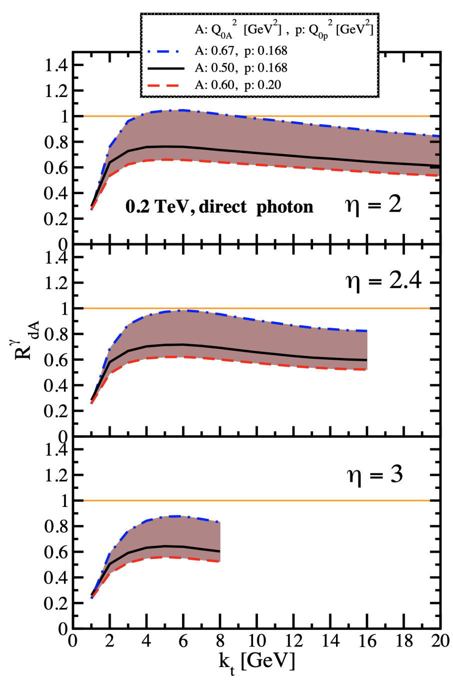

Figure 40: Nuclear modification factor for direct photon production in $p(d)$+A collisions at various rapidities at RHIC $\sqrt{s} = 200$ GeV. The curves are the results obtained from Eq. (12) in Ref. [133] and the solution to rcBK equation using different initial saturation scales for a proton Q_{op} and a nucleus Q_{oA}. The band shows our theoretical uncertainties arising from allowing a variation of the initial saturation scale of the nucleus in a range consistent with previous studies of DIS structure functions as well as particle production in minimum-bias p+p, p+A and A+A collisions in the CGC formalism, see Ref. [133] for details.

collisions, these complications can be ameliorated by removing the strong interaction from the final state, by using photons and Drell-Yan electrons. The Run-15 p+Au run will for the first time provide data on R_{pA} for direct photons and therefore allow one to test CGC based predictions on this observable as depicted in Fig. 40 (taken from Ref. [133]). The higher delivered integrated luminosity for the upcoming Run-24/25 p+Au together with the Forward Upgrade will enable one to study more luminosity hungry processes and/or complementary probes to the di-π^0 correlations, i.e. di-hadron correlations for charged hadrons, photon-jet, photon-hadron and di-jet correlations, which will allow a rigorous test of the calculation in the CGC formalism. It is important to stress that the comparison of these correlation probes in p+p and p+Au requires approximately equal nucleon-nucleon luminosities for these two collision systems for optimal measurements. It is noted that these results are crucial for the equivalent measurements at the EIC, which are planned at close to identical kinematics, because only if non-linear effects are seen with different complementary probes, i.e., e+A and p+A one can claim a discovery of saturation effects and their universality. Therefore it is imperative that analysis activities related to the unpolarized Cold-QCD program continue to be supported throughout the upcoming years.

Direct photon plus jet (direct γ+jet) events can be used as an example channel to indicate what can be done in Run-24/25. These events are dominantly produced through the gluon Compton scattering process, $g + q \rightarrow \gamma + q$, and are sensitive to the gluon densities of the nucleon and nuclei in p+p and p+A collisions. Through measurements of the azimuthal correlations in p+A collisions for direct γ+jet production, one can study non-linear effects at small-x. Unlike di-jet production that is governed by both the Weizsäcker-Williams and dipole gluon densities, direct γ+jet production only accesses the dipole gluon density, which is better understood theoretically [133, 136]. On the other hand, direct γ+jet production is experimentally more challenging due to its small cross-section and large background contribution from di-jet events in which photons from fragmentation or hadron decay could be misidentified as direct photons. The feasibility to perform direct γ+jet measurements with the Forward Upgrade in unpolarized p+p and p+Au collisions at $\sqrt{s_{\rm NN}} = 200$ GeV has been studied. PYTHIA-8.189 [137] was used to produce direct γ+jet and di-jet events. In order to suppress the di-jet background, the leading photon and jet are required to be balanced in transverse momentum, $|\phi^{\gamma} - \phi^{jet}| > 2\pi/3$ and $0.5 < p_T^{\gamma}/p_T^{jet} < 2$. Both the photon and jet have to be in the forward acceptance $1.3 < \eta < 4.0$ with $p_T > 3.2$ GeV/c in 200 GeV p+p collisions. The photon needs to be isolated from other particle activities by requiring the fraction of electromagnetic energy deposition in the cone of $\Delta R = 0.1$ around the photon is more than 95% of that in the cone of $\Delta R = 0.5$. Jets are reconstructed by an anti-k_T algorithm with $\Delta R = 0.5$. After applying these selection cuts, the signal-to-background ratio is around 3:1 [138]. The expected number of selected direct γ+jet events is around ~ 0.9M at $\sqrt{s_{\rm NN}} = 200$ GeV in p+Au collisions for the proposed Run-24. We conclude that a measurement of direct photon-jet correlation from p+Au collisions is feasible, which is sensitive to the gluon density in $0.001 < x < 0.005$ in the Au nucleus where parton saturation is expected.

There are other potential opportunities with the upcoming p+Au and p+p runs that can provide a clean baseline for studying the gluon saturation phenomena in Au+Au using ultra-peripheral collisions (UPC). For example, one of the most powerful measurements proposed at the EIC for discovery of gluon saturation is to look at the double ratio between a heavy nucleus and proton in terms of diffractive processes, see details in Sec. 4.1.3. With STAR Run-24/25, the p+Au UPC (also applies to p+p UPC) may provide two important measurements, e.g., exclusive and inclusive J/ψ production off the proton target, which will serve as a baseline for no saturation. The same measurement will be performed in Au+Au UPC with Run-20 and 25. The different system comparison with STAR data may provide strong evidence for gluon saturation.

4.2.3 sPHENIX

If p+A running will be available for the sPHENIX running period there are several measurements that are planned:

- Measurements of nuclear PDFs [139] via the extractions of neutral pion, jet and direct photon cross sections as a function of transverse momentum and their ratios to p+p collisions. Depending on the final state, the ratios between these cross sections either directly relate to the nuclear PDFs or, in the case of final-state hadrons a convolution with nuclear FFs.

- A particularly clean process to access nuclear PDFs is DY production as no fragmentation contributes. Given the excellent tracking capabilities that are particularly optimized for di-electron measurements for Υ production, di-electron Drell Yan measurements in p+p and p+A collisions will be feasible, making use of the streaming readout.

- Extraction of nuclear fragmentation functions by measuring the fractional momentum dependence of hadrons relative to the momentum of the jet they contribute to. These can be obtained both for p+A and p+p collisions and their comparison would nearly directly single out the nuclear effects of fragmentation.

- Even without p+A collision data, another important measurement in p+p collision data would be the extraction of cross sections for various baryons, particularly for charmed baryons, where the LHC experiments found an excess of particles produced compared to expectations from FFs and the hard interactions. This will be uniquely enabled at RHIC by the sPHENIX heavy-flavor measurement capabilities. The LHCb experiment found that this excess might be only present for higher-multiplicity events [140] and as such studying these cross sections in sPHENIX as a function of multiplicity would help confirm this.

- With inclusive jets, sPHENIX plans to study 2-point energy correlators (EEC), which in p+p collisions provide a clean observable to image jet fragmentation in vacuum. In p+A collisions, EEC are expected to offer insight into CNM effects and how the presence of cold nuclear matter modifies the hadronization mechanism. With Λ-tagged jets, EECs are expected to offer insight into how spin polarization in the initial state is transferred to the final state, and how Λ polarization develops in fragmentation in unpolarized collisions.

5 Data Production

In the following we describe the existing data sets for PHENIX, STAR and sPHENIX and their readiness for analysis and the efforts needed to

5.1 PHENIX

Table 3 summarizes PHENIX data collected from 2006 until the last PHENIX data taking run in 2016. All data sets are fully calibrated and produced enabling the ongoing and future physics analyses. The ongoing efforts for data and analysis preservation (DAP) ensure data and analysis tools availability for active analysers and newcomers in years to come.

Year	$\sqrt{s}$ (GeV)	Recorded Luminosity longitudinally / transverse	Collision System	<P> in %
2006	62.4	0.08 pb^{-1} / 0.02 pb^{-1}	p+p	48
	200	7.5 pb^{-1} / 2.7 pb^{-1}	p+p	57
2008	200	– pb^{-1} / 5.2 pb^{-1}	p+p	45
	200	80 nb^{-1}	d+Au	–
2009	200	16 pb^{-1} /–pb^{-1}	p+p	55
	500	14 pb^{-1} / – pb^{-1}	p+p	39
2011	500	18 pb^{-1} / – pb^{-1}	p+p	48
2012	200	– pb^{-1} / 9.7 pb^{-1}	p+p	61/56
	510	32 pb^{-1} / – pb^{-1}	p+p	50/53
2013	510	155 pb^{-1} / – pb^{-1}	p+p	51/52
2015	200	– pb^{-1} / 60 pb^{-1}	p+p	58
	200	– pb^{-1} / 0.5 pb^{-1}	p+Al	58
	200	– pb^{-1} / 0.2 pb^{-1}	p+Au	61
2016	200	50 nb^{-1}	d+Au	–
	62	5 nb^{-1}	d+Au	–
	39	2 nb^{-1}	d+Au	–
	19	0.1 nb^{-1}	d+Au	–

Table 3: Recorded luminosities for collisions of longitudinally and transversely polarized beams for the different collision systems at the indicated center-of-mass energies for the RHIC runs since 2006. The numbers are for $|vtx| < 30$cm. The average beam polarization as measured by the Hydrogen-jet polarimeter, two polarization numbers are given if the average polarization for the two beams was different

5.2 STAR

Year	$\sqrt{s}$ (GeV)	Recorded Luminosity longitudinally / transverse	Collision System	<P> in %
2006	62.4	– pb^{-1} / 0.2 pb^{-1}	p+p	48
	200	6.8 pb^{-1} / 8.5 pb^{-1}	p+p	57
2008	200	– pb^{-1} / 7.8 pb^{-1}	p+p	45
	200	61 nb^{-1}	d+Au	–
2009	200	25pb^{-1} /–pb^{-1}	p+p	55
	500	10 pb^{-1} / – pb^{-1}	p+p	39
2011	500	12pb^{-1} /25pb^{-1}	p+p	48
2012	200	– pb^{-1} / 22 pb^{-1}	p+p	61/56
	510	82 pb^{-1} / – pb^{-1}	p+p	50/53
2013	510	300 pb^{-1} / – pb^{-1}	p+p	51/52
2015	200	52 pb^{-1} / 52 pb^{-1}	p+p	53/57
	200	– pb^{-1} / 1 pb^{-1}	p+Al	54
	200	– pb^{-1} / 0.45 pb^{-1}	p+Au	60
2016	200	94 nb^{-1}	d+Au	–
	62	15 nb^{-1}	d+Au	–
	39	9.7 nb^{-1}	d+Au	–
	20	2.0 nb^{-1}	d+Au	–
2017	510	– pb^{-1} / 320 pb^{-1}	p+p	55
2022	510	– pb^{-1} / 400 pb^{-1}	p+p	52
2024	200	– pb^{-1} / XX pb^{-1}	p+p	
202X	200	– pb^{-1} / XX pb^{-1}	p+Au	

Table 4: Recorded luminosities for collisions of longitudinally and transversely polarized beams for the different collision systems at the indicated center-of-mass energies for the RHIC runs since 2006. The average beam polarization as measured by the Hydrogen-jet polarimeter, two polarization numbers are given if the average polarization for the two beams was different

Existing data from the STAR experiment covering a broad range of datasets collected over multiple years are listed in Tab. 4. The wealth of these datasets collected over decades of operation provides an invaluable resource for ongoing and future scientific programs. Maintaining this data not only ensures the continuity and integrity of long-term research projects but also enhances the potential for new discoveries as analysis techniques evolve. The primary requirements for producing the existing data at STAR and the essential efforts needed to maintain its quality and accessibility include detector calibration, software development, and the provisioning of computing resources.

Most datasets recorded by the STAR experiment between 2006 and 2017 have been fully calibrated and produced. Those from 2022 and the upcoming 2024 datasets require more meticulous calibration before full production due to the inclusion of new detector systems and increased luminosity. Since 2017, STAR has undergone several important detector upgrades.

At mid-rapidity, the inner Time Projection Chamber (iTPC) was replaced in 2019, enhancing particle identification capabilities and expanding tracking coverage to a pseudorapidity of $|\eta| < 1.5$. At forward rapidity, the Forward Silicon Tracker (FST), the Forward small-strip Thin gap chamber Tracker (FTT), and the Forward Calorimeter System (FCS) were fully installed prior to Run 22. These new systems bring new capabilities and challenges, extending the kinematic coverage into regions that have rarely been probed before. With these new detectors, we have successfully recorded high-quality data at 510 GeV from transversely polarized $p + p$ collisions in 2022 and look forward to similarly successful recording of the 200 GeV dataset in 2024. Precise calibration and integration of these systems are crucial for the accurate reconstruction and analysis of collision events, ensuring that the measurements are both precise and reproducible, and it is critical for conducting high-precision physics analyses.

At mid-rapidity, the calibration of the STAR Time Projection Chamber (TPC) and the Barrel Electromagnetic Calorimeter (BEMC) holds significant importance for numerous physics analysis efforts conducted by the STAR Spin working group. The space-charge (SC) calibration serves as the final crucial step in TPC calibration, addressing distortions arising from ionization within the STAR TPC. Initiated at the onset of this year, this service task commenced with a small test sample and is scheduled for expansion to encompass the entire Run 22 data-taking period. The calibration of the BEMC is currently underway utilizing a preliminary sample with imperfect SC corrections, and will be proceeded to full calibration once the comprehensive TPC SC calibration is completed. The calibration of EEMC is also ongoing and is based on the energy deposition of the minimum ionizing particles (MIPs) from a specific EMC triggered data that were taken during the runs. These calibrations will be ready by the end of 2024. The uncertainty of the calibration for BEMC is 3.5% and it is 4.6% for EEMC. Better calibration results may be possible for EEMC with the extended charge particle tracking from iTPC. Similar calibration processes for the TPC, BEMC, and EEMC are also necessary for the data recorded during Run 24, ensuring consistency and precision in our analyses across different runs.

At forward-rapidity, the new detector systems significantly expand the kinematic coverage of the STAR experiment and enhances its capabilities to probe rare and complex QCD physics. The successful integration of these detectors is crucial to ensure robust and accurate calibration of both tracking and calorimeter detectors. Good alignment between each tracking detector and the forward calorimeter systems not only optimizes individual performance but also improves the overall calibration of the forward calorimeters. The calibration process for the forward calorimeters utilize the analysis of MIPs and π^0 particles reconstructed from Run 22 data. The calibrations began with a small subset of data, with plans to process approximately 20% of the total data from Run 22. This initial phase aims to refine and optimize the tracking algorithms before proceeding to full production.

Software development and maintenance are crucial for converting and preserving all data in standardized formats, ensuring compatibility with both current and prospective analysis software. Continuously updating and developing these software tools is vital for both data production and physics analysis, and also ensures compatibility with evolving software and hardware systems. Significant progress has been made in the reconstruction software for the forward detector systems. These software programs will be tested and refined using the Run 22 preview production data. The production data adhere to the traditional STAR data format known as Micro-DST, abbreviated as MuDST, which requires substantial disk space for storage. For instance, Run 17 utilized approximately 2.7 PB of disk space, and it is anticipated that even more will be needed for Run 22 and Run 24 data productions. Since 2018, the PicoDST data format has been introduced as another standard for STAR experimental data and analysis software. Produced from MuDST, PicoDST retains only the data essential for physics analysis, discarding much of the detailed detector data preserved by MuDST. The streamlined nature of PicoDST files significantly reduces their size, facilitating easier distribution and processing. Software development and integration are needed to encode data from the EEMC and forward detectors into the PicoDST data format, enhancing the efficiency of data management and analysis.

The data production process at STAR is a computationally intensive task, challenged by both the limitations of existing resources and the increasing complexity and volume of data. The full production of Run 17 data required approximately six months, while recently, processing 20% of the Run 22 preview production took about four months. This bottleneck significantly slows the pace of research and limits the potential for timely scientific output. Robust computing resources are crucial for the success of STAR experiment's data production goals. These resources are vital not only for meeting current data production demands but also for supporting future analyses, thereby ensuring the continued success and impact of our experiments. Based on these considerations, it is anticipated that the data production for Run22 at STAR will roughly get completed by the end of 2025.

Embedding simulations are crucial for the STAR experiment as they allow for the detailed analysis of detector performance and particle interactions within the simulated detector environment. Pythia6 with STAR tuned Perugia2012 has proven to be highly effective in describing various aspects of proton+proton collision events at mid-rapidity, including jet production, hadronization within jets, and characteristics of the underlying event across both 200 and 510 GeV collisions. Given this established proficiency, it is anticipated that the production of embedding samples at mid-rapidity for Run22 can be efficiently accomplished in 2026.

The introduction of new detector technologies at forward rapidity has amplified the need for more detailed and extensively tuned simulation samples. These samples are critical for assessing the performance of the detectors and for ensuring that the simulated data accurately reflect the experimental conditions. For Run22, this tuning process will utilize the low luminosity data collected at forward rapidity during the run. Using these samples, critical measurements such as hadron or jet cross sections will be conducted, and the tuning parameters will be refined based on these results. The production of embedding samples at forward rapidity is a time-intensive endeavor, involving iterative cycles of simulation, data comparison, and subsequent adjustments. Depending on the complexity of the detector interactions and the availability of computational resources, each cycle may span several weeks to months.

5.3 sPHENIX

Year	$\sqrt{s}$ (GeV)	Recorded Luminosity transverse	Collision System	<P> in %
2024	200	XX nb^{-1}	p+p	XXX
202X	200	XX nb^{-1}	p+Au	XXX

Table 5: Possible data sets with sPHENIX for collisions with transversely polarized protons.

The possible data sets collected with sPHENIX including at least one beam of transversely polarized protons are listed in Tab. 5. During sPHENIX data production, raw data from all sPHENIX tracking, calorimeter, and global detectors are combined into mini DSTs (mDSTs). To that end, events are assembled from multiple input streams as part of a multi-pass reconstruction that includes calibrations and space-charge distortion corrections for the TPC data. The sPHENIX tracking reconstruction software is based on an adapted version of the "A Common Tracking Software" (ACTS) package. The raw data are processed at SDCC at BNL [141]. Physics data analyses are carried out with mDSTs as input using the C^{++}-/ROOT-based PHENIX user framework Fun4All adapted to sPHENIX.

The resulting timelines to complete the analyses as detailed in Sec. 3.2.3 and Tab. 1 are as follows, considering the time required for commissioning, calibrations, cluster, track, and jet reconstruction and data productions.

The required computing power to produce the 2024 data (more than 50k CPU cores equivalent) and disk-space are already available and are expected to slightly increase by the end of 2024. The final productions of the 2024 data are expected by the end of 2024. Updated/final calibrations will be applied at the analysis stage.

Publications from the 2024 data-taking which use EMCal-only signatures are expected in 2025, starting with the standard candle of the transverse single-spin asymmetry in neutral-meson production, followed by those in direct-photon production. Charged tracks are expected for physics analysis in 2024 after the evaluation of the tracking-detector performances has been completed. The reconstruction of heavy-flavor tracks and calculation of the DCA is expected to be fully developed in 2025. Jet reconstruction with well-calibrated energy scale and controlled uncertainties is expected for 2025 as well. A separation of tracks stemming from the decays of heavy-flavor hadrons into charm and bottom categories will be carried out in 2026. Cold-QCD-related publications with signatures of inclusive jets, photon-jet, or charged tracks are expected for 2026; those with heavy flavor, or hadrons-in-jets for 2027.

6 Appendix

6.1 STAR Forward Upgrade

The STAR forward upgrade consists of four major new subsystems, an electromagnetic calorimeter, a hadronic calorimeter and a tracking system, formed from a silicon detector and a small-strip Thin Gap Chambers tracking detector. It has superior detection capabilities for neutral pions, photons, electrons, jets, and leading hadrons within the pseudorapidity range $2.5 < \eta < 4$, see Fig. 41. The construction of the electromagnetic and hadronic calorimeters was successfully completed by the end of 2020. They were fully installed, instrumented, and commissioned during the 2021 RHIC running period. The tracking detectors were installed in summer and fall 2021, on schedule and ready for the start of Run-22. Note that the entire construction, installation, and commissioning of the four systems were completed in the pandemic period. Enormous efforts were made to keep the forward upgrades on schedule. During Run-22, despite all the difficulties from the machine side, the forward upgrades performed exceptionally well and took data smoothly throughout the run. The forward upgrades will continue taking data in parallel with sPHENIX through Run-25.

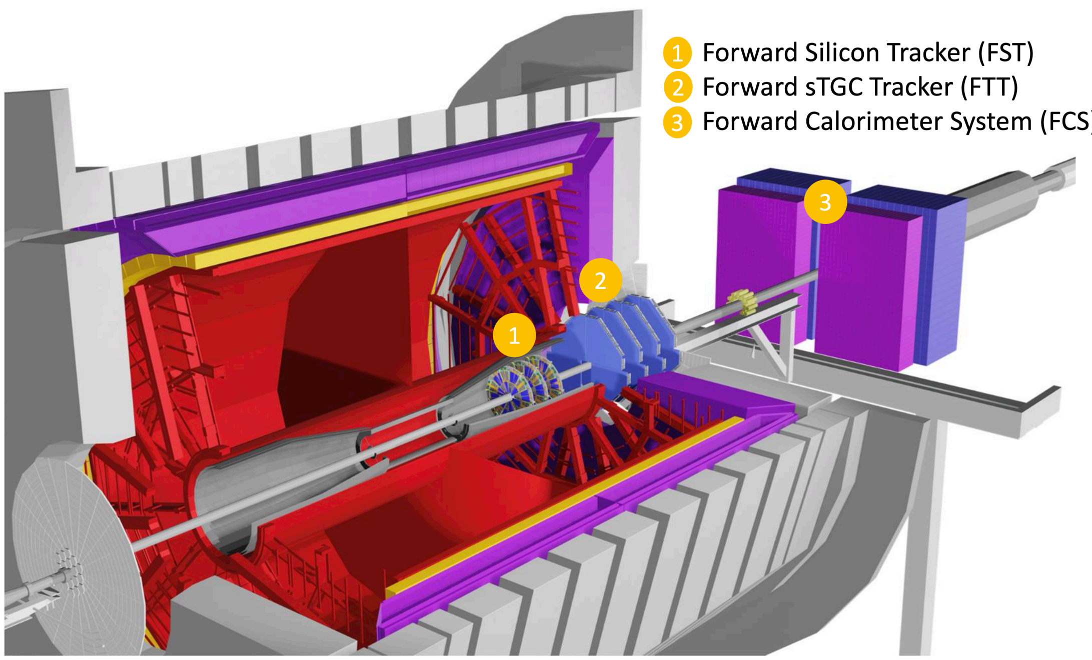

Figure 41: STAR detector with Forward Upgrades

- Forward Calorimeter System:

  The Forward Calorimeter System (FCS) consists of an Electro-Magnetic Calorimeter (Ecal) with 1486 towers, and a Hadronic Calorimeter (Hcal) with 520 towers. All SiPM sensors, front-end electronics boards and readout & triggering boards called DEP were installed, commissioned and calibrated during Run-21. Signal splitter boards for the west EPD detector were installed before Run-22, and the west EPD was used as pre-shower detector in the electron triggers. FPGA code for FCS triggers was developed in fall 2021, and total of 29 triggers, including triggers for electrons, di-electrons, jets, di-jets, hadrons, and photons were commissioned and verified within a few days of RHIC starting to deliver stable $p+p$ collisions, and then used for data taking throughout Run-22 successfully. FCS operations during Run-22 were successful and smooth. The only minor exceptions were 3 low-voltage power supply modules needing to be replaced, and occasional power cycling of electronics being needed due to beam related radiation upsets in the electronics. All 1486 channels of Ecal worked with no bad channels, and the Hcal had only a couple of dead channels. Radiation damage to the SiPM sensors due to beam was within expectations. There was an unexpected loss of signal amplitudes of $\sim$20% per week in the Ecal near the beam, which turned out to be radiation damage in the front-end electronics boards. The loss of signal was compensated during Run-22 by changing the gain factors on the DEP boards, attenuator settings in the front-end electronics, and raising the voltage settings tower by tower based on LED signals.

- Small-strip Thin Gap Chambers:

  The sTGC has four identical planes, each plane has four identical pentagonal shaped gas chambers. These gas chambers are made of double-sided and diagonal strips that give x,y,u in each plane. Sixteen chambers and about 5 spare chambers were built at Shandong University in China. A custom designed and fabricated aluminum frame allowed to fit the detector inside the pole-tip of the STAR magnet and around the beam-pipe on the west side of STAR. The sTGC chambers are operated with a quenching gas mixture of n-Pentane and CO_2 at a ratio of 45%:55% by volume at a typical high voltage of 2900 V. This gas mixture allowed the chambers to operate in a high amplification mode. The sTGC was fully installed prior to the start of Run-22, and the detector was fully commissioned during the first few weeks of the run. The operating point of the high voltage was scanned for optimum efficiency. The gas chambers were stable at the desired operational high voltage and at the high luminosity, also the leakage current was well within the operational limits. In-house, a newly designed and built gas system for mixing, and supplying the gas along a long-heated path to deliver to the chambers, met the above requirements, and performed exceptionally well during Run-22.

- Forward Silicon Tracker:

  The Forward Silicon Tracker (FST) consists of three identical disks, and each disk contains 12 modules. Each module has 3 single-sided double-metal Silicon mini-strips

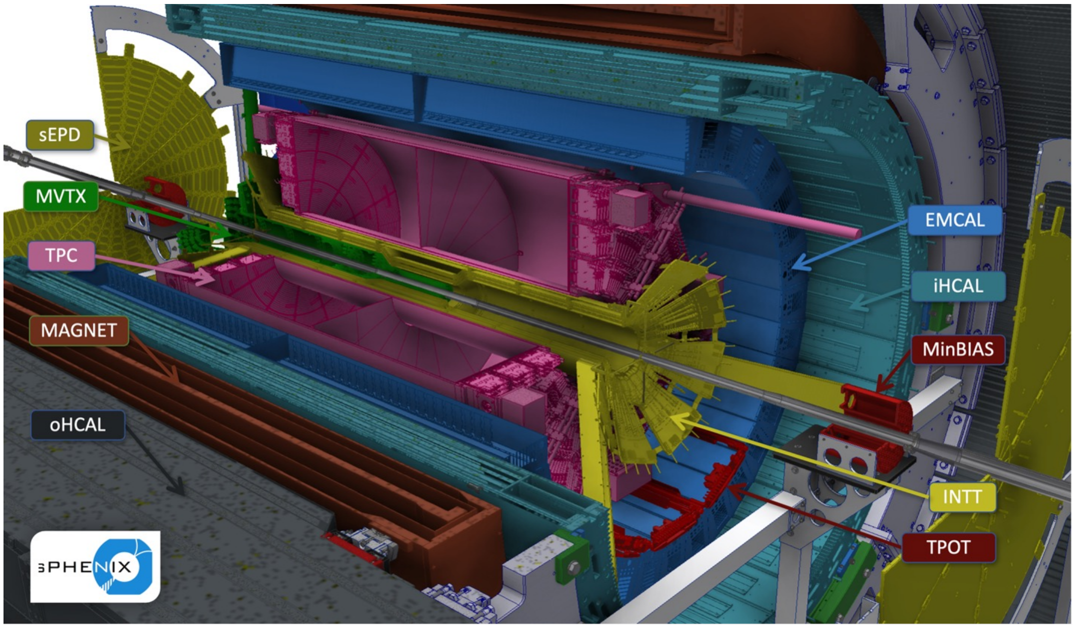

Figure 42: sPHENIX detector layout.

sensors which are read out by 8 APV chips. The module production was done by NCKU, UIC, and SDU. The readout was done by BNL and IU. The cooling was provided by NCKU and BNL. The installation of the FST was completed on August 13th, 2021, and the first p+p 510 GeV collision data were recorded on December 15, 2021. The FST ran smoothly through the whole Run-22, and the detector operation via slow control software was minimal to the shift crew.

6.2 sPHENIX Detector

sPHENIX is a major upgrade to the PHENIX experiment at RHIC capable of measuring jets, photons, charged hadrons, and heavy flavor probes. sPHENIX will play a critical role in the completion of the RHIC science mission, focused on the studies of the microscopic nature of Quark-Gluon Plasma. Polarized proton collisions as well as proton-nucleus collisions will also provide key opportunities for cold QCD measurements.

sPHENIX is a central rapidity detector ($|\eta| < 1.1$) built around the Babar solenoid with magnetic field up to 1.5T. The major systems are a high precision tracking system, and electromagnetic and hadronic calorimeters, see Fig. 42.

The electromagnetic calorimeter is a compact tungsten-scintillating fiber design located inside the solenoid. The outer hadronic calorimeter consists of steel in which scintillator tiles with light collected by wavelength shifting fibers are sandwiched between tapered absorber plates that project nearly radially from the interaction point. It also serves as a flux return of the 1.5 T superconducting solenoid. The inner HCal is instrumented with scintillating tiles similar to the tiles used in the Outer HCal, and serves as a support structure of the electromagnetic calorimeter. The calorimeters use a common set of silicon photomultiplier photodetectors and amplifier and digitizer electronics. Based on test beam data, such a calorimeter system is expected to provide the energy resolution of $\sigma_E/E = 13\%/\sqrt{E[GeV]} \oplus 3\%$ for electromagnetic showers, and $\sigma_E/E = 65\%/\sqrt{E[GeV]} \oplus 14\%$ for hadrons.

The central tracking system consists of a small Time Projection Chamber (TPC), micro vertex detector (MVTX) with three layers of Monolithic Active Pixel Sensors (MAPS), and two layers of the intermediate silicon strip tracker within the inner radius (INTT). Such a system provides momentum resolution $\sigma_{pT}/p_T < 0.2\% \cdot p_T \oplus 1\%$ for p_T =0.2–40 GeV/c, and Distance of Closest Approach (DCA) resolved at 10 μm for $p_T > 2$ GeV/c. The INTT with its fast integration time resolves beam crossings and provides pileup suppression.

The other sPHENIX subsystems are the Minimum Bias Detector (MBD) consisting of the refurbished PHENIX Beam-Beam Counter, Event Plane Detector (sEPD) consisting of two wheels of scintillator tiles positioned at $2 < |\eta| < 4.9$ and serving for event plane measurements, and Micromegas-based TPC Outer Tracker (TPOT), offering calibration of beam-induced space charge distortions in TPC.

High speed data acquisition system is designed to be capable of taking minimum bias *AuAu* collisions at 15 kHz with greater than 90% live time, and jet and photon triggers for *pp* and *pA* operation. The DAQ system is design to be capable to work in hybrid mode: along with triggered data it will collect a significant fraction ($\sim$ 10%) of all collision data from tracking detectors in streaming readout regime, which will greatly extend physics program in *pp* and *pAu* running.

6.3 RHIC SPIN Publications

1. The RHIC Cold QCD Program White Paper: Contribution to the NSAC Long-Range Planning process, E.C. Aschenauer et al., arXiv:2302.00605

2. The RHIC Cold QCD Plan for 2017 to 2023: A Portal to the EIC, E.C. Aschenauer et al., arXiv:1602.03922

3. The RHIC Spin Program: Achievements and Future Opportunities, E.C. Aschenauer et al., arXiv:1501.01220

4. The RHIC Spin Program: Achievements and Future Opportunities, E.C. Aschenauer et al., arXiv:1304.0079

5. Plans for the RHIC Spin Physics Program G. Bunce et al., http://www.bnl.gov/npp/docs/RHICst08_notes/spinplan08_really_final_060908.pdf

PHENIX:

1. Transverse single-spin asymmetry of midrapidity $\pi 0$ and η mesons in p+Au and p+Al collisions at $\sqrt{s_{NN}}$=200 GeV. PHENIX Collaboration, Phys. Rev. D107 (2023) 112004

2. Transverse single-spin asymmetry of charged hadrons at forward and backward rapidity in polarized p+p, p+Al, and p+Au collisions at $\sqrt{s_{NN}}$=200 GeV. PHENIX Collaboration, Phys. Rev. D108 (2023) 072016

3. Improving constraints on gluon spin-momentum correlations in transversely polarized protons via midrapidity open-heavy-flavor electrons in p↑+p collisions at $\sqrt{s}$=200 GeV. PHENIX Collaboration, Phys. Rev. D107 (2023) 052012

4. Measurement of Direct-Photon Cross Section and Double-Helicity Asymmetry at $\sqrt{s}$=510 GeV in p+p Collisions. PHENIX Collaboration, Phys. Rev. Lett. 130 (2023) 251901

5. Transverse-single-spin asymmetries of charged pions at midrapidity in transversely polarized p+p collisions at $\sqrt{s}$ = 200 GeV. PHENIX Collaboration, Phys. Rev. D105 (2022) 032003

6. Transverse single spin asymmetries of forward neutrons in $p + p$, p+Al and p+Au collisions at $\sqrt{s_{_{NN}}}$ = 200 GeV as a function of transverse and longitudinal momenta. PHENIX Collaboration, Phys. Rev. D105 (2022) 032004

7. Probing Gluon Spin-Momentum Correlations in Transversely Polarized Protons through Midrapidity Isolated Direct Photons in $p^{\uparrow}+p$ Collisions at $\sqrt{s}$=200 GeV. PHENIX Collaboration, Phys. Rev. Lett. 127 (2021) 162001

8. Transverse single-spin asymmetries of midrapidity π^0 and η mesons in polarized $p + p$ collisions at $\sqrt{s}$ = 200 GeV. PHENIX Collaboration, Phys. Rev. D103 (2021) 052009

9. Transverse momentum dependent forward neutron single spin asymmetries in transversely polarized p+p collisions at $\sqrt{s}$ = 200 GeV. PHENIX Collaboration, Phys. Rev. D103 (2021) 032007

10. Polarization and cross section of midrapidity J/ψ production in $p + p$ collisions at $\sqrt{s}$ = 510 GeV. PHENIX Collaboration, Phys. Rev. D102 (2020) 072008

11. Measurement of charged pion double spin asymmetries at midrapidity in longitudinally polarized $p + p$ collisions at $\sqrt{s}$ = 510 GeV. PHENIX Collaboration, Phys. Rev. D102 (2020) 032001

12. Nuclear Dependence of the Transverse Single-Spin Asymmetry in the Production of Charged Hadrons at Forward Rapidity in Polarized $p + p$, p+Al, and p+Au Collisions at $\sqrt{s_{_{NN}}}$ = 200 GeV. PHENIX Collaboration, Phys. Rev. Lett. 123 (2019) 122001

13. Nonperturbative transverse momentum broadening in dihadron angular correlations in $\sqrt{s_{NN}}$ = 200 GeV proton-nucleus collisions. PHENIX Collaboration, Phys. Rev. C99 (2019) 044912

14. Nonperturbative transverse-momentum-dependent effects in dihadron and direct photon-hadron angular correlations in $p+p$ collisions at $\sqrt{s} = 200$ GeV. PHENIX Collaboration, Phys. Rev. D98 (2018) 072004

15. Single-spin asymmetry of J/ψ production in $p+p$, p+Al, and p+Au collisions with transversely polarized proton beams at $\sqrt{s_{NN}} = 200$ GeV. PHENIX Collaboration, Phys. Rev. D98 (2018) 012006

16. Cross section and longitudinal single-spin asymmetry A_L for forward $W^\pm \rightarrow \mu^\pm \nu$ production in polarized $p+p$ collisions at $\sqrt{s} = 510$ GeV. PHENIX Collaboration, Phys. Rev. D98 (2018) 032007

17. Nuclear Dependence of the Transverse-Single-Spin Asymmetry for Forward Neutron Production in Polarized $p+A$ Collisions at $\sqrt{s_{NN}}$=200 GeV. PHENIX Collaboration, Phys. Rev. Lett. 120 (2018) 022001

18. Cross section and transverse single-spin asymmetry of muons from open heavy-flavor decays in polarized p+p collisions at $\sqrt{s} = 200$ GeV. PHENIX Collaboration, Phys. Rev. D95 (2017) 112001

19. Angular decay coefficients of J/ψ mesons at forward rapidity from $p+p$ collisions at $\sqrt{s} = 510$ GeV. PHENIX Collaboration, Phys. Rev. D95 (2017) 092003

20. Nonperturbative-transverse-momentum effects and evolution in dihadron and direct photon-hadron angular correlations in $p+p$ collisions at $\sqrt{s}$=510 GeV. PHENIX Collaboration, Phys. Rev. D95 (2017) 072002

21. Measurements of double-helicity asymmetries in inclusive J/ψ production in longitudinally polarized $p+p$ collisions at $\sqrt{s} = 510$ GeV. PHENIX Collaboration, Phys. Rev. D94 (2016) 112008

22. Inclusive cross section and double-helicity asymmetry for π^0 production at midrapidity in $p+p$ collisions at $\sqrt{s} = 510$ GeV. PHENIX Collaboration, Phys. Rev. D93, (2016) 011501. Citations: 73

23. Measurement of parity-violating spin asymmetries in $W^\pm$ production at midrapidity in longitudinally polarized $p+p$ collisions. PHENIX Collaboration, Phys. Rev. D93 (2016) 051103. Citations: 52

24. Charged-pion cross sections and double-helicity asymmetries in polarized p+p collisions at $\sqrt{s}$=200 GeV. PHENIX Collaboration, Phys. Rev. D91 (2015) 032001

25. Cross Section and Transverse Single-Spin Asymmetry of η-Mesons in p$\uparrow$+p Collisions at $\sqrt{s}$=200 GeV at Forward Rapidity. PHENIX Collaboration, Phys. Rev. D90 (2014) 072008. Citations: 53

26. Inclusive double-helicity asymmetries in neutral-pion and eta-meson production in $\vec{p}+\vec{p}$ collisions at $\sqrt{s}$ = 200 GeV. PHENIX Collaboration, Phys.Rev. D90 (2014) 012007. Citations: 112

27. Measurement of transverse-single-spin asymmetries for midrapidity and forward-rapidity production of hadrons in polarized p+p collisions at $\sqrt{s}$ =200 and 62.4 GeV. PHENIX Collaboration, Phys. Rev. D90 (2014) 012006. Citations: 120

28. Inclusive cross section and single transverse spin asymmetry for very forward neutron production in polarized p+p collisions at $\sqrt{s}$=200 GeV. PHENIX Collaboration, Phys.Rev. D88 (2013) 3, 032006.

29. Double Spin Asymmetry of Electrons from Heavy Flavor Decays in $p+p$ Collisions at $\sqrt{s}$ = 200 GeV. PHENIX Collaboration, Phys.Rev. D87 (2013) 012011.

30. Double Spin Asymmetry of Electrons from Heavy Flavor Decays in $p+p$ Collisions at $\sqrt{s}$ = 200 GeV. PHENIX Collaboration, Phys.Rev. D86 (2012) 072008.

31. Cross sections and double-helicity asymmetries of midrapidity inclusive charged hadrons in $p+p$ collisions at $\sqrt{s}$ = 62.4 GeV. PHENIX Collaboration, Phys.Rev. D86 (2012) 092006.

32. Cross section and Parity Violating Spin Asymmetries of $W^{\pm}$ Boson Production in Polarized p+p Collisions at $\sqrt{s}$ = 500 GeV. PHENIX Collaboration, Phys.Rev.Lett. 106 (2011) 062001. Citations: 104

33. Event Structure and Double Helicity Asymmetry in Jet Production from Polarized p+p Collisions at $\sqrt{s}$ = 200 GeV. PHENIX Collaboration, Phys.Rev. D84 (2011) 012006.

34. Measurement of Transverse Single-Spin Asymmetries for J/ψ Production in Polarized p+p Collisions at $\sqrt{s}$ = 200 GeV. PHENIX Collaboration, Phys.Rev. D82 (2010) 112008, Erratum-ibid. D86 (2012) 099904. Citations: 56

35. Cross section and double helicity asymmetry for η mesons and their comparison to neutral pion production in p+p collisions at $\sqrt{s}$ = 200 GeV. PHENIX Collaboration, Phys.Rev. D83 (2011) 032001. Citations: 74

36. Double-Helicity Dependence of Jet Properties from Dihadrons in Longitudinally Polarized p+p Collisions at $\sqrt{s}$ = 200 GeV. PHENIX Collaboration, Phys.Rev. D81 (2010) 012002.

37. The Polarized gluon contribution to the proton spin from the double helicity asymmetry in inclusive π^0 production in polarized p+p collisions at $\sqrt{s}$=200 GeV. PHENIX Collaboration, Phys.Rev.Lett. 103 (2009) 012003. Citations: 137

38. Inclusive cross section and double helicity asymmetry for π^0 production in p+p collisions at $\sqrt{s}$=62.4 GeV. PHENIX Collaboration, Phys.Rev. D79 (2009) 012003. Citations: 136

39. Inclusive cross-Section and double helicity asymmetry for π^0 production in p+p collisions at $\sqrt{s}$=200 GeV: Implications for the polarized gluon distribution in the proton. PHENIX Collaboration, Phys.Rev. D76 (2007) 051106. Citations: 290

40. Measurement of direct photon production in p + p collisions at $\sqrt{s}$ = 200-GeV. PHENIX Collaboration, Phys.Rev.Lett. 98 (2007) 012002. Citations: 212

41. Improved measurement of double helicity asymmetry in inclusive midrapidity π^0 production for polarized p+p collisions at $\sqrt{s}$=200 GeV. PHENIX Collaboration, Phys.Rev. D73 (2006) 091102.

42. Measurement of transverse single-spin asymmetries for mid-rapidity production of neutral pions and charged hadrons in polarized p+p collisions at $\sqrt{s}$=200 GeV. PHENIX Collaboration, Phys.Rev.Lett. 95 (2005) 202001. Citations: 207

43. Mid-rapidity direct-photon production in p^+p collisions at $\sqrt{s}$ = 200-GeV. PHENIX Collaboration, Phys.Rev. D71 (2005) 071102. Citations: 59

44. Double helicity asymmetry in inclusive mid-rapidity π^0 production for polarized p+p collisions at $\sqrt{s}$=200 GeV. PHENIX Collaboration , Phys.Rev.Lett. 93 (2004) 202002. Citations: 91

45. Mid-rapidity neutral pion production in proton proton collisions at $\sqrt{s}$ = 200-GeV PHENIX Collaboration, Phys.Rev.Lett. 91 (2003) 241803. Citations: 396

STAR:

1. Results on Elastic Cross Sections in Proton-Proton Collisions at $\sqrt{s}$ = 510 GeV with the STAR Detector at RHIC, Phys. Lett. B 852 (2024) 138601

2. Exclusive J/Psi, Psi(2s), and e^+e^- pair production in Au+Au ultra-peripheral collisions at RHIC, submitted for publication, arxiv: 2311.13632

3. Observation of strong nuclear suppression in exclusive J/Psi photoproduction in Au+Au ultraperipheral collisions at RHIC, arxiv: 2311.13637, accepted for publication in Phys. Rev. C

4. Measurements of Z^0 cross section and transverse single spin asymmetry of Z^0 in 500/510 GeV p+p collisions. STAR Collaboration, accepted for publication for Phys. Lett. B, arxiv:2308.15496

5. Measurement of transverse single-spin asymmetries for dijet production in polarized proton-proton collisions at $\sqrt{s}$ = 200 GeV. STAR Collaboration, submitted for publication, arxiv:2305.10359

6. Longitudinal and transverse spin transfer to Lambda and anti-Lambda hyperons in polarized $p+p$ collisions at $\sqrt{s} = 200$ GeV. STAR Collaboration, Phys. Rev. D 109 (2024) 12004

7. Azimuthal transverse single-spin asymmetries of inclusive jets and identified hadrons within jets from polarized pp collisions at $\sqrt{s} = 200$ GeV. STAR Collaboration, Phys. Rev. D 106 (2022) 72010

8. Evidence for Nonlinear Gluon Effects in QCD and Their Mass Number Dependence at STAR. STAR Collaboration, Phys. Rev. Lett. 129 (2022) 092501

9. Longitudinal double-spin asymmetry for inclusive jet and dijet production in polarized proton collisions at $\sqrt{s} = 510$ GeV. STAR Collaboration, Phys. Rev. D 105 (2022) 92011, citations: 27

10. Longitudinal double-spin asymmetry for inclusive jet and dijet production in polarized proton collisions at $\sqrt{s} = 200$ GeV. STAR Collaboration, Phys. Rev. D 103 (2021) L091103, citations: 27

11. Comparison of transverse single-spin asymmetries for forward π^0 production in polarized pp, pAl and pAu collisions at nucleon pair c.m. energy $\sqrt{s} = 200$ GeV. STAR Collaboration, Phys. Rev. D 103 (2021) 72005

12. Measurement of transverse single-spin asymmetries of π^0 and electromagnetic jets at forward rapidity in 200 and 500 GeV transversely polarized proton-proton collisions. STAR Collaboration, Phys. Rev. D 103 (2021) 92009, citations: 31

13. Measurements of W and Z/γ Cross Section and Cross-Section Ratios in $p+p$ Collisions at RHIC. STAR Collaboration, Phys. Rev. D 103 (2021) 012001

14. Longitudinal double spin asymmetry for inclusive jet and dijet production in pp collisions at $\sqrt{s} = 510$ GeV. STAR Collaboration, Phys. Rev. D 100 (2019) 052005, citations: 59

15. Measurement of the longitudinal spin asymmetries for weak boson production in proton-proton collisions at $\sqrt{s} = 510$ GeV. STAR Collaboration, Phys. Rev. D 99 (2019) 051102, citations: 33

16. Transverse spin transfer to Lambda and anti-Lambda hyperons in polarized proton-proton collisions at $\sqrt{s} = 200$ GeV. STAR Collaboration, Phys. Rev. D 98 (2018) 091103

17. Improved measurement of the longitudinal spin transfer to Lambda and Anti-Lambda hyperons in polarized proton-proton collisions at $\sqrt{s} = 200$ GeV. STAR Collaboration, Phys. Rev. D 98 (2018) 112009

18. Longitudinal Double-Spin Asymmetries for Dijet Production at Intermediate Pseudorapidity in Polarized pp Collisions at $\sqrt{s} = 200$ GeV. STAR Collaboration, Phys. Rev. D 98 (2018) 032011, citations: 32

19. Longitudinal double-spin asymmetries for π^0's in the forward direction for 510 GeV polarized pp collisions. STAR Collaboration, Phys. Rev. D 98 (2018) 032013, citations: 27

20. Transverse spin-dependent azimuthal correlations of charged pion pairs measured in p+p collisions at $\sqrt{s} = 500$ GeV. STAR Collaboration, Phys. Lett. B 780 (2018) 332-339, citations: 29

21. Azimuthal transverse single-spin asymmetries of inclusive jets and charged pions within jets from polarized-proton collisions at $\sqrt{s} = 500$ GeV. STAR Collaboration, Phys. Rev. D 97 (2018) 32004, citations: 42

22. Measurement of the cross section and longitudinal double-spin asymmetry for di-jet production in polarized $p{+}p$ collisions at $\sqrt{s} = 200$ GeV. STAR Collaboration, Phys. Rev. D 95 (2017) 71103 citations: 47

23. Measurement of the transverse single-spin asymmetry in $p^{\uparrow}{+}p \rightarrow W^{\pm}/Z^0$ at RHIC. STAR Collaboration, Phys.Rev.Lett. 116 (2016) 132301, citations: 129

24. Observation of Transverse Spin-Dependent Azimuthal Correlations of Charged Pion Pairs in $p^{\uparrow}{+}p$ at $\sqrt{s} = 200$ GeV. STAR Collaboration, Phys.Rev.Lett. 115 (2015) 242501, citations: 49

25. Precision Measurement of the Longitudinal Double-spin Asymmetry for Inclusive Jet Production in Polarized Proton Collisions at $\sqrt{s} = 200$ GeV. STAR Collaboration, Phys. Rev. Lett. 115 (2015) 092002, citations: 162

26. Measurement of longitudinal spin asymmetries for weak boson production in polarized proton-proton collisions at RHIC. STAR Collaboration, Phys.Rev.Lett. 113 (2014) 072301, citations: 103

27. Neutral pion cross section and spin asymmetries at intermediate pseudorapidity in polarized proton collisions at $\sqrt{s} = 200$ GeV. STAR Collaboration, Phys. Rev. D 89 (2014) 012001, citations: 50

28. Single Spin Asymmetry A_N in Polarized Proton-Proton Elastic Scattering at $\sqrt{s} = 200$ GeV. STAR Collaboration, Phys. Lett. B 719 (2013) 62, citations: 76

29. Transverse Single-Spin Asymmetry and Cross-Section for π^0 and η Mesons at Large Feynman-x in Polarized $p{+}p$ Collisions at $\sqrt{s} = 200$ GeV. STAR Collaboration, Phys. Rev. D 86 (2012) 51101, citations: 102

30. Longitudinal and transverse spin asymmetries for inclusive jet production at mid-rapidity in polarized p+p collisions at $\sqrt{s} = 200$ GeV. STAR Collaboration, Phys. Rev. D 86 (2012) 32006, citations: 113

31. Measurement of the $W \to e^{+}\nu$ and $Z/\gamma \to e^{+} + e^{-}$ Production Cross Sections at Mid-rapidity in Proton-Proton Collisions at $\sqrt{s} = 500$ GeV. STAR Collaboration, Phys. Rev. D 85 (2012) 92010, citations: 42

32. Measurement of the parity-violating longitudinal single-spin asymmetry for $W^{\pm}$ boson production in polarized proton-proton collisions at $\sqrt{s} = 500$ GeV. STAR Collaboration, Phys. Rev. Lett. 106 (2011) 62002, Citations: 95

33. Longitudinal double-spin asymmetry and cross section for inclusive neutral pion production at midrapidity in polarized proton collisions at $\sqrt{s} = 200$ GeV. STAR Collaboration, Phys.Rev. D80 (2009) 111108, citations: 69

34. Longitudinal Spin Transfer to Lambda and anti-Lambda Hyperons in Polarized Proton-Proton Collisions at $\sqrt{s} = 200$ GeV. STAR Collaboration, Phys.Rev. D80 (2009) 111102, citations: 29

35. Forward Neutral Pion Transverse Single Spin Asymmetries in p+p Collisions at $\sqrt{s} = 200$ GeV. STAR Collaboration, Phys.Rev.Lett. 101 (2008) 222001, citations: 226

36. Longitudinal double-spin asymmetry for inclusive jet production in p+p collisions at $\sqrt{s} = 200$ GeV. STAR Collaboration, Phys.Rev.Lett. 100 (2008) 232003, citations: 154

37. Measurement of transverse single-spin asymmetries for di-jet production in proton-proton collisions at $\sqrt{s} = 200$ GeV. STAR Collaboration, Phys.Rev.Lett. 99 (2007) 142003, citations: 64

38. Longitudinal double-spin asymmetry and cross section for inclusive jet production in polarized proton collisions at $\sqrt{s} = 200$ GeV. STAR Collaboration, Phys.Rev.Lett. 97 (2006) 252001, citations: 257

39. Cross-Sections and transverse single spin asymmetries in forward neutral pion production from proton collisions at $sqrts = 200$ GeV. STAR Collaboration, Phys.Rev.Lett. 92 (2004) 171801, citations: 373

References

[1] DSSV, D. de Florian, R. Sassot, M. Stratmann, and W. Vogelsang, Phys. Rev. Lett. **113**, 012001 (2014).

[2] DSSV Preliminary.

[3] STAR Collaboration, M. M. Aggarwal *et al.*, Phys. Rev. Lett. **106**, 062002 (2011), 1009.0326.

[4] PHENIX Collaboration, A. Adare *et al.*, Phys. Rev. Lett. **106**, 062001 (2011), 1009.0505.

[5] STAR Collaboration, L. Adamczyk *et al.*, Phys. Rev. Lett. **113**, 072301 (2014), 1404.6880.

[6] PHENIX Collaboration, A. Adare *et al.*, Phys. Rev. D **93**, 051103 (2016), 1504.07451.

[7] PHENIX Collaboration, A. Adare *et al.*, Phys. Rev. D **98**, 032007 (2018), 1804.04181.

[8] STAR Collaboration, J. Adam *et al.*, Phys. Rev. D **99**, 051102 (2019), 1812.04817.

[9] D. de Florian, R. Sassot, M. Stratmann, and W. Vogelsang, Phys. Rev. Lett. **113**, 012001 (2014).

[10] NNPDF, E. R. Nocera, R. D. Ball, S. Forte, G. Ridolfi, and J. Rojo, Nucl. Phys. B **887**, 276 (2014), 1406.5539.

[11] STAR Collaboration, J. Adam *et al.*, Phys. Rev. D **98**, 032011 (2018).

[12] STAR Collaboration, J. Adam *et al.*, Phys. Rev. D **100**, 052005 (2019).

[13] STAR Collaboration, M. S. Abdallah *et al.*, Phys. Rev. D **103**, L091103 (2021), 2103.05571.

[14] STAR Collaboration, M. S. Abdallah *et al.*, Phys. Rev. D **105**, 092011 (2022), 2110.11020.

[15] STAR Collaboration, N. Lukow, Constraining the Polarized Gluon Distribution Function of the Proton with Recent STAR Measurements, in *24th International Spin Symposium*, 2021.

[16] PHENIX Collaboration, A. Adare *et al.*, Phys. Rev. D **93**, 011501 (2016).

[17] PHENIX Collaboration, U. A. Acharya *et al.*, Phys. Rev. D **102**, 032001 (2020), 2004.02681.

[18] STAR Collaboration, B. I. Abelev *et al.*, Phys. Rev. Lett. **97**, 252001 (2006).

[19] STAR Collaboration, B. I. Abelev *et al.*, Phys. Rev. Lett. **100**, 232003 (2008).

[20] STAR Collaboration, L. Adamczyk *et al.*, Phys. Rev. D **86**, 032006 (2012).

[21] STAR Collaboration, L. Adamczyk *et al.*, Phys. Rev. Lett. **115**, 092002 (2015).

[22] STAR Collaboration, L. Adamczyk *et al.*, Phys. Rev. D **95**, 071103 (2017).

[23] PHENIX Collaboration, A. Adare *et al.*, Phys. Rev. D **76**, 051106 (2007).

[24] PHENIX Collaboration, A. Adare *et al.*, Phys. Rev. Lett. **103**, 012003 (2009).

[25] PHENIX Collaboration, A. Adare *et al.*, Phys. Rev. D **79**, 012003 (2009).

[26] STAR Collaboration, B. Abelev *et al.*, Phys. Rev. D **80**, 111108 (2009).

[27] STAR Collaboration, L. Adamczyk *et al.*, Phys. Rev. D **89**, 012001 (2014).

[28] PHENIX Collaboration, A. Adare *et al.*, Phys. Rev. D **90**, 012007 (2014).

[29] STAR Collaboration, J. Adam *et al.*, Phys. Rev. D **98**, 032013 (2018).

[30] PHENIX Collaboration, A. Adare *et al.*, Phys. Rev. D **91**, 032001 (2015), 1409.1907.

[31] PHENIX Collaboration, U. Acharya *et al.*, Phys. Rev. Lett. **130**, 251901 (2023), 2202.08158.

[32] DSSV, D. de Florian, G. A. Lucero, R. Sassot, M. Stratmann, and W. Vogelsang, Phys. Rev. D **100**, 114027 (2019).

[33] STAR, J. Kwasizur, Longitudinal Double-Spin Asymmetries for Dijet Production at Intermediate Pseudorapidity in Polarized Proton-Proton Collisions at $\sqrt{s} = 510$ GeV, in *APS Division of Nuclear Physics Meeting*, 2020.

[34] Jefferson Lab Angular Momentum (JAM), Y. Zhou, N. Sato, and W. Melnitchouk, Phys. Rev. D **105**, 074022 (2022), 2201.02075.

[35] PHENIX, A. Adare *et al.*, Phys. Rev. D **90**, 072008 (2014), 1406.3541.

[36] STAR Collaboration, M. Abdallah *et al.*, Phys. Rev. D **106**, 072010 (2022), 2205.11800.

[37] U. D'Alesio, F. Murgia, and C. Pisano, Phys. Lett. B **773**, 300 (2017), 1707.00914.

[38] Z.-B. Kang, X. Liu, F. Ringer, and H. Xing, JHEP **11**, 068 (2017), 1705.08443.

[39] Z.-B. Kang, A. Prokudin, F. Ringer, and F. Yuan, Phys. Lett. B **774**, 635 (2017), 1707.00913.

[40] U. D'Alesio, F. Murgia, and C. Pisano, Phys. Rev. D **83**, 034021 (2011), 1011.2692.

[41] STAR Collaboration, L. Adamczyk *et al.*, Phys. Rev. D **97**, 032004 (2018), 1708.07080.

[42] STAR, H. Liu, Measurement of transverse single-spin asymmetries for dijet production in polarized *pp* collisions at $\sqrt{s} = 200$ GeV at STAR, in *Nuclear Physics Seminar, Brookhaven National Laboratory*, 2020, https://indico.bnl.gov/event/8633/.

[43] J. Collins and J.-W. Qiu, Phys. Rev. D **75**, 114014 (2007).

[44] T. C. Rogers and P. J. Mulders, Phys. Rev. D **81**, 094006 (2010).

[45] X. Liu, F. Ringer, W. Vogelsang, and F. Yuan, Phys. Rev. D **102**, 114012 (2020), 2008.03666.

[46] Z.-B. Kang, K. Lee, D. Y. Shao, and J. Terry, JHEP **02**, 066 (2021), 2008.05470.

[47] STAR Collaboration, L. Adamczyk *et al.*, Phys. Rev. Lett. **115**, 242501 (2015), 1504.00415.

[48] STAR Collaboration, L. Adamczyk *et al.*, Phys. Lett. B **780**, 332 (2018), 1710.10215.

[49] M. Radici and A. Bacchetta, Phys. Rev. Lett. **120**, 192001 (2018), 1802.05212.

[50] STAR Collaboration, J. Adam *et al.*, Phys. Rev. D **103**, 092009 (2021), 2012.11428.

[51] STAR Collaboration, J. Adam *et al.*, Phys. Rev. D **103**, 072005 (2021), 2012.07146.

[52] STAR, *Transverse Single Spin Asymmetry for Inclusive and Diffractive Electromagnetic Jets at Forward Rapidities in* $p^{\uparrow}p$ *Collisions at* $\sqrt{s} = 200$ *GeV and 510 GeV at STAR*, Zenodo, 2022.

[53] M. Boglione *et al.*, Phys. Lett. B **815**, 136135 (2021), 2101.03955.

[54] RHIC-f Collaboration, M. H. Kim *et al.*, Phys. Rev. Lett. **124**, 252501 (2020), 2003.04283.

[55] H.-J. Kim, S. Clymton, and H.-C. Kim, Phys. Rev. D **106**, 054001 (2022), 2206.02184.

[56] STAR, S. Collaboration, (2023), 2308.15496.

[57] M. Bury, A. Prokudin, and A. Vladimirov, JHEP **05**, 151 (2021), 2103.03270.

[58] M. Bury, A. Prokudin, and A. Vladimirov, Phys. Rev. Lett. **126**, 112002 (2021), 2012.05135.

[59] A. Bacchetta, F. Delcarro, C. Pisano, and M. Radici, Phys. Lett. B **827**, 136961 (2022), 2004.14278.

[60] PHENIX Collaboration, U. A. Acharya *et al.*, Phys. Rev. Lett. **127**, 162001 (2021).

[61] K. Kanazawa, Y. Koike, A. Metz, and D. Pitonyak, Phys. Rev. D **91**, 014013 (2015).

[62] Y. Koike and S. Yoshida, Phys. Rev. D **85**, 034030 (2012).

[63] PHENIX Collaboration, N. J. Abdulameer *et al.*, Phys. Rev. D **107**, 052012 (2023), 2204.12899.

[64] Z.-B. Kang, J.-W. Qiu, W. Vogelsang, and F. Yuan, Phys. Rev. D **78**, 114013 (2008), 0810.3333.

[65] Y. Koike and S. Yoshida, Phys. Rev. D **84**, 014026 (2011), 1104.3943.

[66] D. M. Hofman and J. Maldacena, Journal of High Energy Physics **2008**, 012 (2008).

[67] H. Chen, I. Moult, X. Zhang, and H. X. Zhu, Phys. Rev. D **102**, 054012 (2020).

[68] P. T. Komiske, I. Moult, J. Thaler, and H. X. Zhu, Phys. Rev. Lett. **130**, 051901 (2023).

[69] Z.-B. Kang, K. Lee, D. Y. Shao, and F. Zhao, (2023), 2310.15159.

[70] Jefferson Lab Angular Momentum (JAM), C. Cocuzza *et al.*, Phys. Rev. D **109**, 034024 (2024), 2308.14857.

[71] COMPASS Collaboration, G. D. Alexeev *et al.*, High-statistics measurement of Collins and Sivers asymmetries for transversely polarised deuterons, 2024, 2401.00309 and acc. Phys. Rev. Lett.

[72] Belle, A. Vossen *et al.*, Phys. Rev. Lett. **107**, 072004 (2011), 1104.2425.

[73] Belle, R. Seidl *et al.*, Phys. Rev. D **96**, 032005 (2017), 1706.08348.

[74] JAM, C. Cocuzza *et al.*, Phys. Rev. Lett. **132**, 091901 (2024), 2306.12998.

[75] Jefferson Lab Angular Momentum, J. Cammarota *et al.*, Phys. Rev. D **102**, 054002 (2020), 2002.08384.

[76] HERMES, A. Airapetian *et al.*, Phys. Lett. B **577**, 37 (2003), hep-ex/0307023.

[77] HERMES, A. Airapetian *et al.*, Nucl. Phys. B **780**, 1 (2007), 0704.3270.

[78] HERMES, A. Airapetian *et al.*, Phys. Lett. B **684**, 114 (2010), 0906.2478.

[79] W. Brooks and H. Hakobyan, Nucl. Phys. A **830**, 361C (2009), 0907.4606.

[80] NuSea, M. Vasilev *et al.*, Phys. Rev. Lett. **83**, 2304 (1999), hep-ex/9906010.

[81] K. J. Eskola, P. Paakkinen, H. Paukkunen, and C. A. Salgado, Epps21: A global qcd analysis of nuclear pdfs, 2021.

[82] PHENIX, S. Adler *et al.*, Phys. Rev. Lett. **98**, 172302 (2007), nucl-ex/0610036.

[83] R. Sassot, M. Stratmann, and P. Zurita, Phys. Rev. D **81**, 054001 (2010), 0912.1311.

[84] E. Aschenauer *et al.*, (2014), 1409.1633.

[85] N. Armesto, H. Paukkunen, J. M. PenÃn, C. A. Salgado, and P. Zurita, Eur. Phys. J. C **76**, 218 (2016), 1512.01528.

[86] H. Paukkunen, K. J. Eskola, and C. Salgado, Nucl. Phys. A **931**, 331 (2014), 1408.4563.

[87] K. J. Eskola, H. Paukkunen, and C. A. Salgado, JHEP **10**, 213 (2013), 1308.6733.

[88] H. Paukkunen and P. Zurita, JHEP **12**, 100 (2014), 1402.6623.

[89] V. Guzey and M. Klasen, Phys. Rev. D **104**, 114013 (2021), 2012.13277.

[90] L. Gribov, E. Levin, and M. Ryskin, Phys. Rept. **100**, 1 (1983).

[91] E. Iancu and R. Venugopalan, The Color glass condensate and high-energy scattering in QCD, in *In *Hwa, R.C. (ed.) et al.: Quark gluon plasma* 249-3363*, 2003, hep-ph/0303204.

[92] H. Weigert, Prog. Part. Nucl. Phys. **55**, 461 (2005), hep-ph/0501087.

[93] J. Jalilian-Marian and Y. V. Kovchegov, Prog. Part. Nucl. Phys. **56**, 104 (2006), hep-ph/0505052.

[94] F. Gelis, E. Iancu, J. Jalilian-Marian, and R. Venugopalan, Ann. Rev. Nucl. Part. Sci. **60**, 463 (2010), 1002.0333.

[95] G. Giuliani, H. Zheng, and A. Bonasera, Prog. Part. Nucl. Phys. **76**, 116 (2014), 1311.1811.

[96] Y. V. Kovchegov and E. Levin, *Quantum Chromodynamics at High Energy*Cambridge Monographs on Particle Physics, Nuclear Physics and Cosmology (Cambridge University Press, 2012).

[97] A. H. Mueller and J.-w. Qiu, Nucl. Phys. B **268**, 427 (1986).

[98] L. McLerran and R. Venugopalan, Phys. Rev. D **49**, 2233 (1994).

[99] L. McLerran and R. Venugopalan, Phys. Rev. D **49**, 3352 (1994).

[100] L. McLerran and R. Venugopalan, Phys. Rev. D **50**, 2225 (1994).

[101] Y. V. Kovchegov, Phys. Rev. D **54**, 5463 (1996).

[102] Y. V. Kovchegov, Phys. Rev. D **55**, 5445 (1997).

[103] J. Jalilian-Marian, A. Kovner, L. McLerran, and H. Weigert, Phys. Rev. D **55**, 5414 (1997).

[104] A. H. Mueller, Nucl. Phys. **B415**, 373 (1994).

[105] A. H. Mueller and B. Patel, Nucl. Phys. B **425**, 471 (1994), hep-ph/9403256.

[106] I. Balitsky, Nucl. Phys. **B463**, 99 (1996), hep-ph/9509348.

[107] I. Balitsky, Phys. Rev. D **60**, 014020 (1999), hep-ph/9812311.

[108] Y. V. Kovchegov, Phys. Rev. **D60**, 034008 (1999), hep-ph/9901281.

[109] Y. V. Kovchegov, Phys. Rev. D **61**, 074018 (2000), hep-ph/9905214.

[110] J. Jalilian-Marian, A. Kovner, and H. Weigert, Phys. Rev. D **59**, 014015 (1998), hep-ph/9709432.

[111] J. Jalilian-Marian, A. Kovner, A. Leonidov, and H. Weigert, Phys. Rev. D **59**, 014014 (1998), hep-ph/9706377.

[112] E. Iancu, A. Leonidov, and L. D. McLerran, Phys. Lett. B **510**, 133 (2001), hep-ph/0102009.

[113] E. Iancu, A. Leonidov, and L. D. McLerran, Nucl. Phys. **A692**, 583 (2001), hep-ph/0011241.

[114] A. Accardi *et al.*, Eur. Phys. J. A **52**, 268 (2016), 1212.1701.

[115] Y. V. Kovchegov and M. D. Sievert, Nucl. Phys. B **903**, 164 (2016), 1505.01176.

[116] CMS, S. Chatrchyan *et al.*, Eur. Phys. J. C **74**, 2951 (2014), 1401.4433.

[117] STAR, E. Braidot, Nucl. Phys. A **854**, 168 (2011), 1008.3989.

[118] PHENIX Collaboration, A. Adare *et al.*, Phys. Rev. Lett. **107**, 172301 (2011), 1105.5112.

[119] C. Marquet, Nucl. Phys. A **796**, 41 (2007), 0708.0231.

[120] J. L. Albacete and C. Marquet, Phys. Rev. Lett. **105**, 162301 (2010), 1005.4065.

[121] Z.-B. Kang, I. Vitev, and H. Xing, Phys. Rev. D **85**, 054024 (2012), 1112.6021.

[122] M. Strikman and W. Vogelsang, Phys. Rev. D **83**, 034029 (2011), 1009.6123.

[123] STAR Collaboration, M. S. Abdallah *et al.*, Phys. Rev. Lett. **129**, 092501 (2022), 2111.10396.

[124] S. Klein and J. Nystrand, Photoproduction of J/Ψ and Υ in pp and $\bar{p}p$ collisions, in *5th Workshop on Small x and Diffractive Physics*, 2003, hep-ph/0310223.

[125] S. R. Klein, J. Nystrand, J. Seger, Y. Gorbunov, and J. Butterworth, Comput. Phys. Commun. **212**, 258 (2017), 1607.03838.

[126] J. Lansberg, L. Massacrier, L. Szymanowski, and J. Wagner, Phys. Lett. B **793**, 33 (2019), 1812.04553.

[127] PHENIX Collaboration, C. Aidala *et al.*, Phys. Rev. Lett. **123**, 122001 (2019), 1903.07422.

[128] S. Benić and Y. Hatta, Phys. Rev. D **99**, 094012 (2019), 1811.10589.

[129] PHENIX Collaboration, C. Aidala *et al.*, Phys. Rev. Lett. **120**, 022001 (2018), 1703.10941.

[130] PHENIX Collaboration, U. A. Acharya *et al.*, Phys. Rev. D **105**, 032004 (2022), 2110.07504.

[131] B. Z. Kopeliovich, I. K. Potashnikova, I. Schmidt, and J. Soffer, Phys. Rev. D **84**, 114012 (2011), 1109.2500.

[132] G. Mitsuka, Phys. Rev. C **95**, 044908 (2017), 1702.03834.

[133] J. Jalilian-Marian and A. H. Rezaeian, Phys. Rev. D **86**, 034016 (2012), 1204.1319.

[134] J. L. Albacete and C. Marquet, Nucl. Phys. A **854**, 154 (2011), 1009.3215.

[135] K. J. Eskola, H. Paukkunen, and C. A. Salgado, JHEP **07**, 102 (2008), 0802.0139.

[136] A. H. Rezaeian, Phys. Rev. D **86**, 094016 (2012), 1209.0478.

[137] T. Sjostrand, S. Mrenna, and P. Z. Skands, Comput. Phys. Commun. **178**, 852 (2008), 0710.3820.

[138] Di-jet production from pythia8.189 is scaled down due to its overestimation of inclusive π_0 yields compared to those reported by BRAHMS in phys. rev. lett. 98 (2007) 252001 and STAR in phys. rev. lett. 97 (2006) 152302.

[139] I. Helenius, J. Lajoie, J. D. Osborn, P. Paakkinen, and H. Paukkunen, Physical Review D **100** (2019).

[140] LHCb, R. Aaij *et al.*, Phys. Rev. Lett. **131**, 061901 (2023), 2204.13042.

[141] R. Corliss, PoS **ICHEP2022**, 224 (2022).